White Rose Research Online

eprints@whiterose.ac.uk
https://eprints.whiterose.ac.uk
Universities of Leeds, Sheffield and York

Deposited via The University of Sheffield.

White Rose Research Online URL for this paper:
https://eprints.whiterose.ac.uk/id/eprint/240503/

Version: Accepted Version

**Article:**
Rabea, K., Heeley, A., Gheit, A. et al. (2026) High quality, H2-rich syngas production from wood and miscanthus gasification in a novel stationary fluidized bed gasifier: An experimental investigation. Fuel, 424. 139301. ISSN: 0016-2361

https://doi.org/10.1016/j.fuel.2026.139301

© 2026 The Authors. Except as otherwise noted, this author-accepted version of a journal article published in Fuel is made available via the University of Sheffield Research Publications and Copyright Policy under the terms of the Creative Commons Attribution 4.0 International License (CC-BY 4.0), which permits unrestricted use, distribution and reproduction in any medium, provided the original work is properly cited. To view a copy of this licence, visit http://creativecommons.org/licenses/by/4.0/

**Reuse**
This article is distributed under the terms of the Creative Commons Attribution (CC BY) licence. This licence allows you to distribute, remix, tweak, and build upon the work, even commercially, as long as you credit the authors for the original work. More information and the full terms of the licence here: https://creativecommons.org/licenses/

**Takedown**
If you consider content in White Rose Research Online to be in breach of UK law, please notify us by emailing eprints@whiterose.ac.uk including the URL of the record and the reason for the withdrawal request.

UNIVERSITY OF LEEDS
University of Sheffield
UNIVERSITY of York

# High quality, $H_2$-rich syngas production from wood and miscanthus gasification in a novel stationary fluidized bed gasifier: An experimental investigation

Karim Rabea[a,b*], Andy Heeley[a], Abdulaziz Gheit[a], Kris Milkowski[a], Nik Nor Aznizam[a], Karen N. N. Finney[a], Kevin J. Hughes[a], Derek Ingham[a], Mohamed Pourkashanian[a].

a. Energy 2050, Energy Innovation Centre (EIC), Department of Mechanical Engineering, Faculty of Engineering, University of Sheffield, Sheffield, UK.

b. Mechanical Power Engineering Department, Faculty of Engineering, Tanta University, Tanta 31511, Egypt.

## ABSTRACT

Biomass will need to play a major role in the transition towards carbon neutrality in the energy sector. The conversion of biomass into syngas through gasification enables its usage in various applications including combined heat and power generation, production of sustainable hydrocarbon fuels and hydrogen generation. The compromise between producing syngas with both a high calorific value and low tar content remains challenging across various gasifier reactors. The rising co-current gasifier presents a novel reactor design that combines the advantages of the fixed and fluidized bed reactors in terms of the biomass conversion efficiency and quality of syngas produced. However, limited research has been conducted on this design, and its capabilities and limitations have not been characterised fully. This study presents an investigation of the performance of a rising co-current gasifier with two different feedstocks (wood and miscanthus pellets) over a range of operating conditions. The gasifier achieved an optimum balance between achieving a high magnitude of lower heating value (LHV) and a minimum tar content under different operating conditions. The LHV of syngas varied between 5.0 and 5.5 MJ/Nm$^3$ for both materials, with the wood pellets achieving slightly higher values than the miscanthus. The equivalence ratio (ER) is estimated at 0.283-0.287 for wood pellets and at 0.319-0.339 for miscanthus. The gasifier achieved high cold gas efficiency (CGE) and carbon conversion efficiency (CCE), attaining maximum values of 83.1% and 98.0%, respectively. The $H_2$ content in the syngas had a mean value of approximately 18%, with the $H_2$/CO ratio in the range of 0.8-0.9. A minimum tar content of 14.7 mg/Nm$^3$ of syngas was attained from the wood pellets at an air flow rate of 75 kg/h (ER=0.285), while the maximum tar content of 163.5 mg/Nm$^3$, was observed from the gasification of miscanthus pellets at a flow rate of 55 kg/h (ER=0.319). It is worth highlighting that the gasification of miscanthus pellets imposed the additional challenge of bed agglomeration and the formation of channels in the bed, however fluidization at higher air flow rates can, at least in part, mitigate this problem.

## Keywords

35 Biomass; $H_2$-rich syngas; Gasification; Rising co-current; Slag formation; Tar analysis.

36 *Corresponding author. karim_rabea@yahoo.com, k.elamawy@sheffield.ac.uk

# Nomenclature

**Abbreviations**

| | |
|---|---|
| BFB | Bubbling fluidized bed |
| CCE | Carbon conversion efficiency |
| CGE | Cold gas efficiency |
| CV | Calorific value |
| ER | Equivalence ratio |
| FTIR | Fourier transform infrared |
| HHV | Higher heating value |
| ICP-OES | Inductively coupled plasma optical emission spectroscopy |
| LHV | Lower heating value |
| M | Molecular weight |
| *stoich* | Stoichiometric |
| TOC | Total organic carbon |
| TRL | Technology readiness level |
| wt.% | Weight percent |
| XRF | X-ray fluorescence |

**Symbols**

| | |
|---|---|
| $V_g$ | Gas yield ($m^3/kg$) |
| $\dot{m}$ | Mass flow rate |
| $\dot{Q_{air}}$ | Air flow rate ($Nm^3/h$) |
| $N_2$ | mole fraction of Nitrogen in the syngas |
| CO | mole fraction of carbon monoxide in the syngas |
| $CO_2$ | mole fraction of carbon dioxide in the syngas |
| $CH_4$ | mole fraction of methane in the syngas |
| $H_2$ | mole fraction of hydrogen in the syngas |
| $C_nH_m$ | mole fraction of higher hydrocarbons in the syngas |

## 1 Introduction

Climate change, driven by anthropogenic greenhouse gas emissions from fossil fuels, poses an increasing threat to the global ecosystem and human societies, therefore, presenting an urgent need for the transition to renewable and sustainable energy sources [1]. Organic biomass materials such as agricultural residues, forestry by-products and dedicated energy crops, also known as bioenergy, present a promising solution to mitigate climate change. Bioenergy is considered to be a major contributor within the renewable energy matrix for the transition toward a sustainable low-carbon future [1]. Gasification of biomass by thermal decomposition in an oxygen-deficient (sub-stoichiometric) environment is a preferred option for thermochemical conversion of biomass into a gaseous fuel, owing to the high conversion rate of biomass and the versatility of the gas produced [2]. The synthetic gas (syngas) produced can be utilized for combined heat and power applications or further processed to produce sustainable chemicals, hydrocarbon fuels and/or hydrogen [3]. The quality of the syngas depends on many variables, such as the type of gasifier, type of biomass feedstock, and operating conditions [4]. Many gasifier designs and configurations are available, where the nature of the reactor bed (fluidized or fixed) is a primary and distinguishing criterion. Every design has its advantages in terms of their operation and how the initial biomass feedstock affects key parameters, such as syngas calorific value and quality and ash, char and tar content. A persistent challenge is the presence of tar in the syngas which may hinder syngas processing for power generation and/or biofuels production, particularly where the upper acceptable limit of tar content for syngas processing is 0.1 g/Nm$^3$ [5]. This includes the utilisation of syngas as fuel, for example in fuel cells or its conversion into hydrogen, methanol, sustainable aviation fuel, and other gas-to-x applications [5]. Other power generation applications, such as gas turbines, can operate with slightly higher tar contents, although they may still encounter issues, such as condensation onto valve mechanisms and fuel pipelines. Post-generation gas cleaning is often used to provide syngas of

sufficiently low tar and extraneous gas concentrations to afford usability in applications that demand high-purity fuel [6, 7]. Achieving low concentrations of non-combustible gases and tar from the gasification process eases the demands upon post-generation cleaning equipment, affecting capital equipment and operating costs. It is beneficial to operate gasifiers to deliver lower concentrations of these species.

While fluidized bed gasifiers feature improved gas-solid interaction [8], fixed beds are simpler with no need for a fluidization medium and the downsizing of particles. Furthermore, the average tar content from conventional fluidized bed gasifier designs is 10 g/Nm$^3$ [9], which is higher than downdraft fixed bed gasifier configurations [10]. Typically, the tar concentration in the syngas from the gasification of wood pellets in a bubbling fluidized bed (BFB) has been reported to be in the range of 2.22-7.85 g/Nm$^3$, including known and unknown species of tar [11].

The syngas compositions in studies of air-based gasification of wood pellets in pilot BFB gasifier plants by Pio et al [12] and Kim et al [13] had lower heating value (LHV) maxima between 5.6 MJ/Nm$^3$ and 6.1 MJ/Nm$^3$ and molar hydrogen concentrations between 12.7% and 16.5%.

For the case of fixed bed gasifiers, various designs and configurations have been investigated in the literature. For example, a flexible design to achieve different configurations (downdraft, updraft, or dual bed reactor) has been studied for syngas production from woody biomass [14-16]. This was achieved by utilizing different positions of the air inlet, syngas outlet, and ignition port. The syngas from the updraft configuration exhibited a relatively high LHV of 4.8 MJ/Nm$^3$, compared to the dual bed reactor that achieved 4.3 MJ/Nm$^3$ and the downdraft configuration at 3.8 MJ/Nm$^3$ [14-17]. Despite the lower LHV for the downdraft configuration, the tar content in syngas produced from downdraft gasifiers is typically low, ranging between 0.015 and 0.3 g/Nm$^3$ [17]. In contrast, updraft gasifiers produce syngas with significantly higher tar levels, such as 26.9 g/Nm³ for woodchips [18]. Furthermore, in a study by Li et al. [19], a different design of the updraft gasifier was investigated, yielding an LHV of 4.4 MJ/Nm$^3$ for pine wood gasification.

90 The thermal conversion efficiency, also known as cold gas efficiency (CGE), varied according
91 to the gasifier configuration and the feedstock. The CGE for woody biomass gasification in the
92 fixed bed type of gasifiers has been reported between 50-91% [14-16, 18].

93 It is important to highlight that the demand for woody biomass is increasing for many
94 applications, therefore it is important to integrate other biomass sources into the supply chain for
95 generating syngas by gasification and especially the perennial herbaceous ones. Perennial
96 grasses, such as miscanthus, offer a high energy yield compared to other annual crops because
97 their energy content is comparable to woody biomass. These crops are also ecologically benign,
98 having no detrimental effect upon the land upon which they are grown or even beneficial effect
99 through phytoremediation of depleted soils, in some cases [20-22].

100 Miscanthus has shown a high potential to be considered as a biomass feedstock for the
101 gasification process, where high heating value and high thermal and conversion efficiency can
102 be obtained [23]. However, the $H_2$ concentration achieved was relatively low, with volumetric
103 proportions of syngas reported at 10.0 vol.% in the study of Xue et al [23]. In the study by Kallis
104 et al. [24], the $H_2$ content was higher, at 11.3%, from the gasification of miscanthus in a
105 downdraft gasifier, however, the corresponding CGE of 30% was significantly lower than that
106 attained in the Xue et al study (~62%). In another study on miscanthus gasification in a pilot
107 scale, bottom-fired fluidised bed gasifier, the maximum $H_2$ content reported was 11.3 vol.% with
108 a CGE of 58% at an equivalence ratio (ER) of 0.25 [20].

109 Herbaceous biomass tends to contain high levels of ash which presents other concerns about its
110 use as a feedstock in high-temperature gasifiers, predominantly slag formation, which is a major
111 challenge that affects the operation of the gasifier, especially in conventional fluidized bed
112 reactors [25]. Slag is formed when inorganic metals in the ash agglomerate with the bed material
113 (fluidization medium), commonly silica sand, at high temperatures. Bed agglomeration and slag
114 formation cause de-fluidisation of the bed, suppressing solid-gas interactions, thereby reducing

the syngas heating value and fuel ‘quality’. The extent of slag formation is increased when biomass with high Si and alkali/alkali earth metals, such as K, Ca, Na et cetera are present in the ash; when found with other elements, such as Cl and S, the resulting chlorides and sulphates lead to slag formation. The extent of slag formation is increased when biomass with high concentrations of potassium (K) and silicon (Si) in the ash are present. This is attributed to the low melting temperature of the resulting compounds [23].

To reduce tar and slag formation while maintaining the LHV at a high level, a unique concept of gasifier design known as the rising co-current gasifier has emerged. It combines the advantages of both fixed and fluidized bed reactors to achieve optimum performance [26]. Unlike conventional fluidised bed gasifiers, this design uniquely achieves fluidisation of the bed without using any inert fluidisation medium or bed material of any kind. Although the design concept of the gasifier was patented by Klaus Weichselbaum under patent number DE102008043131B4 in 2012 [27], limited research has been undertaken on this design to comprehensively examine and evaluate its performance under different operating conditions with different biomass types to achieve optimum performance while minimising its constraints. Hence, the present study investigates the performance of a pilot scale (approximately 200 $kW_{th}$) rising co-current gasifier, with wood and miscanthus pellet feedstocks representing woody and herbaceous biomass, respectively, aiming to produce high-quality, $H_2$-rich syngas.

This is the first study to explore the gasification of herbaceous biomass using such a gasifier design, including considerations of the effects of the higher ash content compared to wood pellets. The study fully characterizes the pilot-scale gasifier's performance with these feedstocks and enables evaluations of the feasibility of using this gasifier design for different applications, assuming operation at optimal conditions.

## 2 Materials and methods

### 2.1 Feedstock specification

Commercially available wood pellet and miscanthus pellet feedstocks were selected for the biomass gasification process to represent woody and herbaceous biomass types. The specifications of the pellets complied with the "EN Plus A1" standard and should ensure operational stability of the gasifier. The proximate and ultimate analyses as well as the calorific value (CV) measurement were carried out to characterize the feedstocks as presented in Table 1. The proximate and ultimate analyses and the calorific value estimation were performed according to the standard methodologies in laboratories that are accredited to ISO/IEC 17025 UKAS standard [28]. It is worth noting that the fixed carbon and the oxygen were calculated by difference.

Table 1. Biomass feedstock characteristics.

| Analysis | Wood pellets | Miscanthus pellets |
|---|---|---|
| Proximate analysis (wt.% as received) | | |
| Moisture | 7.4 | 9.0 |
| Volatile Matter | 78.2 | 73.6 |
| Fixed Carbon | 13.6 | 14.6 |
| Ash | 0.8 | 2.9 |
| Ultimate analysis (wt.%, dry basis) | | |
| Carbon | 50.5 | 47.8 |
| Hydrogen | 6.8 | 6.5 |
| Nitrogen | 0.1 | 0.3 |
| Oxygen | 41.6 | 42.0 |
| Sulphur/Sulphate | 0.03 | 0.04 |
| Chlorine/Chloride | 0.05 | 0.1 |
| Calorific value (kJ/kg) | | |
| HHV | 18342 | 18272 |
| LHV | 16877 | 16856 |

The bulk densities of the wood and the miscanthus pellets have been evaluated as 653 kg/m$^3$ and 593 kg/m$^3$, respectively. The pellets' dimensions were 6-8 mm diameter and approximately 20 mm length. Additionally, the content of metals in both feedstocks is presented in Fig. 1.

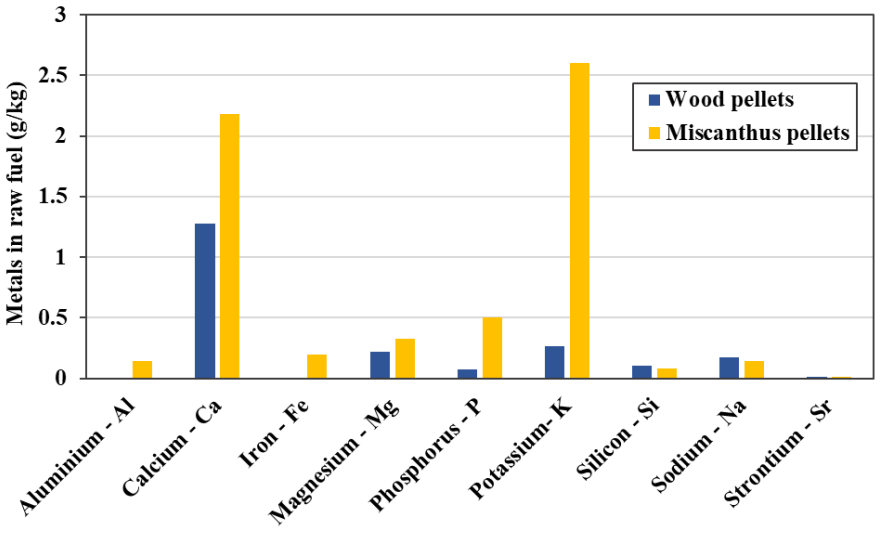


Fig. 1. ICP metals analyses of wood and miscanthus fuel pellets

## 2.2 The rising co-current gasifier

The design concept of the rising co-current gasifier features feeding of both air and biomass to the bottom of the reactor vessel, whilst ignition occurs at the top of the biomass bed. The gasifier is an updraft design following the air flow configuration, but the distribution of the gasification zones resembles that of the downdraft gasifier. These are the drying, pyrolysis, combustion and reduction zones but proceed in an inverted order from the bottom upward as illustrated in Fig. 2. The conversion of biomass into syngas takes place during transit up through the reactor, where the biomass particles decompose as they move through the high-temperature zones. This results in a reduction in the weight and the size of the particles as they progress through the gasification stages, which later enables the fluidization of the top section of the bed, referred to as a static or stationary fluidised bed in which the solid pellets become buoyant in the gas flow and circulate within the section, acting like a BFB without any supplementary bed material needed.

The pilot reactor design comprises a cylindrical section with a diameter of 0.53 m and a height of 0.7 m, on top of a cone-shaped section with a height of 0.6 m and ending with an inlet diameter of 0.25 m to enable feeding of the biomass from the bottom of the reactor. The temperature distribution along the gasifier reactor is monitored simultaneously by 10 k-type thermocouples (T4-T13) located as shown in Fig. 2. The pellets are fed to the reactor by an auger where the feeding control is accomplished based on the feedback signal from the level indicator that is submerged into the bed by 5 cm, also shown in Fig. 2. Air is supplied to the gasifier using a blower and the flow rate is measured using an inline air mass flow meter, adjusted along with the pellet feed rate to ensure the specified air to fuel ratio is achieved and consistent throughout steady-state operation. The hot syngas is cooled by recirculating cooling water in a 3-stage double pipe heat exchanger which cools down the syngas to approximately 140 °C. A very small volume flow of the syngas is drawn off and cooled further for real-time analysis.

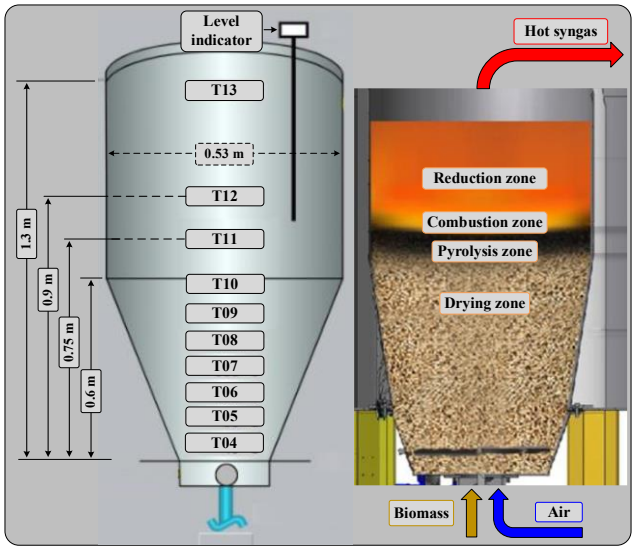


Fig. 2. The rising co-current gasifier geometry, reaction zones and thermocouple locations.

## 2.3 Test conditions

The trial operating conditions used with each fuel type: air flow rates and reactor bed height are presented in Table 2. The bed height is defined as the probe measurement of the packed and

fluidised region of pellets in the reactor, with the tip embedded by 50 mm into the reacting mass of pellets (see level indicator positioning in Fig. 2).

Table 2. Sets of trial operating conditions used during the investigation of co-current gasifier process characterisation with pelletised wood and miscanthus fuels.

| | Wood pellet fuel | | | | | | | | Miscanthus pellet fuel | | | |
|---|---|---|---|---|---|---|---|---|---|---|---|---|
| Air flow rate (kg/h) | 50 | 55 | 60 | 65 | 70 | 75 | 75* | 70* | 66* | 55 | 65 | 75 |
| Reactor bed height (cm) | 85 | 85 | 105 | 85, 95, 105 | 105 | 85 | 90 | 95 | 100 | 85 | 85, 95, 105 | 85 |
| *Test cases under CHP mode; air flow rate is controlled by the CHP at a specified electricity output setpoint where 75, 70 and 66 kg/h represent 50, 45, and 40 kWe, respectively. | | | | | | | | | | | | |

To prepare the gasifier for operation, the reactor was filled with biomass to an approximate level of the required bed height, then the gasifier lid is to be closed and sealed followed by a leakage check by pressurising the system with air and monitoring the pressure drop. The gasifier is ignited from the top of the bed through a dedicated port in the reactor lid which has a quick seal mechanism. The feeding rates of fresh biomass into the reactor is adjusted to maintain the specified bed height at the set point. There are two modes of operation (Flare mode and CHP mode), where a constant air flow rate and bed height are set by the user. These conditions are handled by the control algorithm, which maintain constant airflow (Flare mode) while keeping the bed height at the set point by adjusting the biomass feeding rate accordingly at the specified air flow rate. For the power generation mode (CHP mode), the air supply and consequently the biomass feeding rate are controlled by the CHP demand of syngas with enough energy content. The results of the gasifier operation under CHP control, as well as additional results from the gasifier, are presented in the supplementary material.

## 2.4 Syngas characterisation methodology

The composition of the cold syngas is analysed continuously by the extractive gas analysis unit utilising infrared gas sensors (Flow-Evo, SmartGas, GmbH) for measurement of 0-50 vol.%

CO, 0-20 vol.% $CO_2$ and 0-10 vol.% $CH_4$. The $H_2$ content is measured by a thermal conductivity sensor with a measuring range of 0-100 vol.%.

It is worth highlighting that the $CH_4$ measurement cannot differentiate between gaseous hydrocarbon species and therefore this represents all of the combustible hydrocarbon species in the syngas as a single concentration of methane. Methane would however be the principal hydrocarbon gas species generated anyway and would contribute the most significant component of hydrocarbon calorific value to the syngas. To further analyse the syngas and account for the other trace gases present in the outlet stream, another bleed stream of the syngas was analysed using a standalone FTIR gas analyser (Gasmet DX4000). This analyser covers a wide range of components, with characterisation of the species within the measured spectrum selectable from a library of known spectra. This included water vapour content, hydrocarbons, oxides of carbon, aldehydes and nitrogenous compounds. This more comprehensive analysis of gas species would confirm the proportions of hydrocarbon gases in the syngas, therefore the error introduced by the representation of all hydrocarbon gases as methane was accepted as representative of the hydrocarbon content of syngas for online analysis. Identification of gas species was achieved and concentrations were measured by selecting components that corresponded to the positions of characteristic absorption bands present within the FTIR spectrum and comparing with the spectrum libraries available. The spectrum characterisation was applied to the sample measured continuously during operation of the gasifier, thereby providing near real-time analysis of the gas composition.

The gas sample was drawn at a rate of approximately 5 L/min through a heated sample line to the gas conditioning unit with both set at 180°C to mitigate water vapour condensation. In addition, the oxygen content in the syngas was measured using a separate Zirconia sensor that is located in the heated filter unit through which the gas sample is passed prior to the FTIR analyser.

## 2.5 Tar collection and analysis

A sampling probe was installed in the middle stage of the double-pipe heat exchanger, at which point the gas had cooled to approximately 350°C, to extract a sample for measurement of the tar content in the syngas stream. The gas sample was transferred through a heated line, which was maintained at the same temperature as the gas sampling unit to mitigate condensation of water vapour and tars. The gas was drawn into the tar sampling configuration and the volumetric flow rate was controlled by the Apex Instruments gas sampling equipment. A schematic diagram of the sampling setup is presented in Fig. 3. The tar sampling was carried out according to the standard method of tar sampling and analysis in product gases, CEN/TS 15439:200610 [29]. The gravimetric analysis of tar was accomplished by using a vacuum rotary evaporator and a weighing scale with a resolution of 0.1 mg.

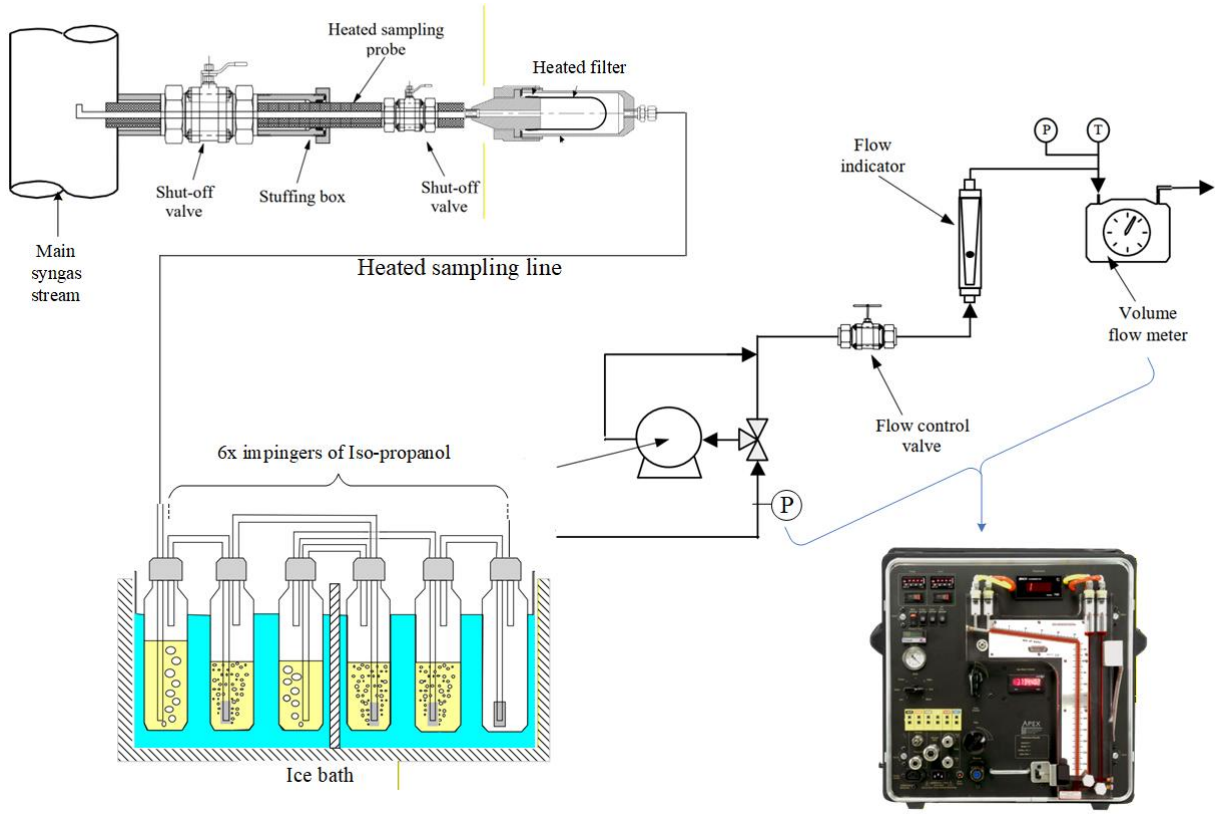


Fig. 3. Flow sheet of the tar sampling setup.

## 2.6 Solid materials analyses

The content of inorganic materials in the slag collected from the gasifier reactor (i.e. from the agglomerated remains of the fluidised fuel pellet bed) and char/ash that was collected from the fabric filter housing, residual solid mass removed from the reactor bed once cooled from operational state and the external waste ash collection bag, were analysed using inductively coupled plasma optical emission spectroscopy (ICP-OES) and X-ray Fluorescence (XRF) techniques. The sample preparation for the ICP-OES analysis was carried out by digesting the sample fine particles using a reverse aqua-regia solvent (hydrochloric acid >37%, and nitric acid 65%) under pressure microwave treatment [30]. This method is suitable for dissolving most of the sample elements but silicates remain undissolved, hence the XRF analysis was conducted on the same set of samples to achieve an accurate assessment of the silica content in the slag..

## 2.7 Process evaluation parameters

The assessment of the gasification process was carried out by estimating the LHV, CGE, syngas yield (Vg), and carbon conversion efficiency (CCE). These were estimated based on the extent of the different compounds in the syngas (i.e., mole fractions of $H_2$, CO, $CH_4$, $C_nH_m$) and the gas yield as shown below [31]:

$$\mathrm{LHV}_{gas}(\mathrm{MJ}/m^3) = [(10.79 \times \mathrm{H_2}) + (12.636 \times \mathrm{CO}) + (35.82 \times \mathrm{CH_4})] \quad (1)$$

$$\mathrm{CGE}\ (\%) = \frac{[\mathrm{LHV}]_{\mathrm{gas}} \times V_g}{[\mathrm{LHV}]_{\mathrm{Biomass}}} \times 100\% \quad (2)$$

$$V_g = \frac{\left(\dot{Q}_{air} \times 0.79\right)}{(\mathrm{N_2} \times \dot{m}_B)} \quad (3)$$

$$\mathrm{CCE}\ (\%)\ = \frac{12 \times (\mathrm{CO} + \mathrm{CO_2} + \mathrm{CH_4} + \sum n[\,\mathrm{C_nH_m}])}{22.4 \times \mathrm{C}} \times V_g \times 100\% \quad (4)$$

where the gas yield, $V_g$ ($Nm^3$/kg of biomass), was evaluated as the ratio of nitrogen mole fraction in the air (assumed as 0.79) and the syngas. Nitrogen is selected due to its nature as an inert gas,

making it a perfect tracer gas. In Equation (3), the only nitrogen introduced to the gasifier is that of the air (at 0.79), while the nitrogen content in the biomass is assumed to be negligible (this assumption has been validated by the elemental analysis, as seen from Table 1. This approach is commonly used in such applications due to the difficulty of operating a mass flow meter with a gas of varying composition during gasifier operation [32]. $\dot{Q}_{air}$ is the air volume flow rate into the gasifier ($Nm^3/h$) and $\dot{m}_B$ is the biomass consumption rate (kg/h). CCE is estimated by comparing the mass flow of carbon in the produced syngas and the mass flow of carbon in the biomass, both normalised to 1 kg of biomass supplied. This is achieved by estimating the volume of carbon-containing compounds in the gas using molar fractions and the gas yield, then converted to a molar flow of carbon using the ideal gas standard molar volume of gas (22.4 $Nm^3/kmol$) before being transformed to a mass flow using the molar mass of carbon (12 kg/kmol). The inlet mass flow of carbon, represented by C (the mass fraction of carbon content in biomass on a dry basis, as determined by the ultimate analysis shown in Table 1). CCE represents a good metric for evaluating the mass balance across the gasifier reactor, particularly when expecting the composition of the char/ash to be dominated by carbon. Furthermore, the Equivalence Ratio (ER), a key parameter for evaluating system performance, reflects how oxygen-deficient the process is. This is achieved by comparing the ratio of the actual air/biomass mass flow rate to the stoichiometric ratio, as shown in equation (5).

$$ER = \frac{\left[\frac{\dot{m}_{air}}{\dot{m}_B}\right]_{act}}{\left[\frac{\dot{m}_{air}}{\dot{m}_B}\right]_{stoich}} \quad (5)$$

where $\dot{m}$ is the mass flow rate (kg/h), and the stoichiometric air to biomass ratio represents the theoretical amount of air that would be required for complete combustion of a unit of biomass, and it can be estimated using equation (5) [32]:

$$\left[\frac{\dot{m}_{air}}{\dot{m}_B}\right]_{stoich} = \frac{1.293}{0.21}\left(1.866\frac{\mathrm{C_{d,a,f}}}{100} + 5.55\frac{\mathrm{H_{d,a,f}}}{100} + 0.7\frac{\mathrm{S_{d,a,f}}}{100} - 0.7\frac{\mathrm{O_{d,a,f}}}{100}\right) \quad (5)$$

such that $C_{d,a,f}$, $H_{d,a,f}$, $S_{d,a,f}$ and $O_{d,a,f}$ are the biomass elemental mass-based composition on dry-ash-free basis, which is the ultimate analysis presented in Table 1.

## 3 Results and discussion

### 3.1 Gasifier performance analysis

The real-time distribution of the reactor temperature and the gas composition, along with the corresponding biomass feeding rate and pressure drop during the gasification of wood pellets and miscanthus pellets at 65 kg/h air flow rate are presented in Fig. 4. Also, the impact of step changing the bed height from 85 to 95 and then to 105 during gasifier operation on its performance is evaluated.

The gasifier is started by igniting the top of the bed (at 85 cm bed height) whilst a low air flow rate of 40 kg/h is supplied to help the ignition front propagate downward until T8 reaches 200 °C. The temperature versus time history of the thermocouple measurements, presented in Fig. 4 (a) and (b), demonstrated this start-up sequence prior to steady operation at different sets of conditions and transient behaviour during changes.

After approximately 40 minutes, the start-up phase was completed and the air flow rate was increased to the reference set point condition of 65 kg/h, after which the syngas analysis was initiated. A reduction in the bed temperature was observed from Fig. 4a and Fig. 4b for both feedstocks after about 1 hour of operation. This was mainly because of the increase in the fresh biomass feeding rate to more than 40 kg/h for both wood pellets and miscanthus pellets, once the gasifier was able to run at its nominal operating set point of air flow rate. This constant feeding at a higher rate than during start-up, as noted in Fig. 4c and Fig. 4d, introduces colder material to the hot section of the bed, where the heat is utilized for drying and pyrolyzing the fresh pellets through endothermic processes, which causes the transient temperature changes.

309 The same phenomenon is repeated whenever a step change in biomass feeding is applied. As a
310 result of these changes in operation, the syngas composition changes, albeit these are transient
311 and the system attains stable operation again at the control set point. The gas composition
312 changes have a slight effect on the calorific value of the syngas because the variations of
313 concentrations of the combustible gases partially compensate for each other, as can be seen for
314 the first 10 hours of operation with both materials presented in Fig. 4e and Fig. 4f.

315 Table 3 presents the average syngas composition over the first 10 hours of operation at an air
316 flow rate of 65 kg/h for both feedstocks. The syngas produced from wood pellets generally has
317 higher concentrations of CO and $H_2$ compared to miscanthus pellets, while miscanthus-derived
318 syngas exhibited a higher $CO_2$ content. Additionally, the $CH_4$ levels were somewhat higher in
319 syngas from wood pellets. This difference in gas composition can be attributed to the
320 characteristics of the feedstocks, specifically that the miscanthus pellets had higher moisture
321 content and lower volatile matter (VM) and carbon content than the wood pellets, as previously
322 presented in Table 1. High moisture content in biomass tends to reduce the CO and $H_2$ content
323 in syngas and increases the $CO_2$ concentration [33]. This can be reversed when the gasifier
324 temperature increases, where the CO and $H_2$ concentrations increase as a result of promoted
325 Boudouard reaction of $CO_2$ as well as the thermal cracking and steam reforming of tar
326 compounds [34]. This can be observed during miscanthus gasification between the 14th and the
327 20th hour of operation (see Fig. 4b and Fig. 4f).

328 A similar effect occurred during wood pellet gasification between the 40th and the 50th hours of
329 operation, where more moisture is released from the fresh feed (represented by the increased
330 temperatures measured by T6 and T7 in Fig. 4a), promoting the steam reforming reaction while
331 the reactor temperature is high (T12). Also, the extent of VM and the carbon content are essential
332 for the production of CO, where a large portion of CO is released during the biomass
333 decomposition phase of the gasification process [35]. Alongside the release of VM, the extent of

carbon in char helps in producing more CO than $CO_2$ through the reduction reaction (Boudouard reaction) and the water-gas reaction [5].

The variability, indicated by the standard deviations (SD) presented in Table 3, suggests that CO and $H_2$ concentrations in syngas from wood pellets were more stable than $CO_2$ and $CH_4$ levels that incurred more variation. In contrast, miscanthus pellets demonstrated slightly less variability across most gas components, reflecting a more consistent syngas composition. These variations were directly related to the changes in the bed temperature, which were affected by the changes in the feeding rates of fresh biomass into the reactor and consequent bed height changes.

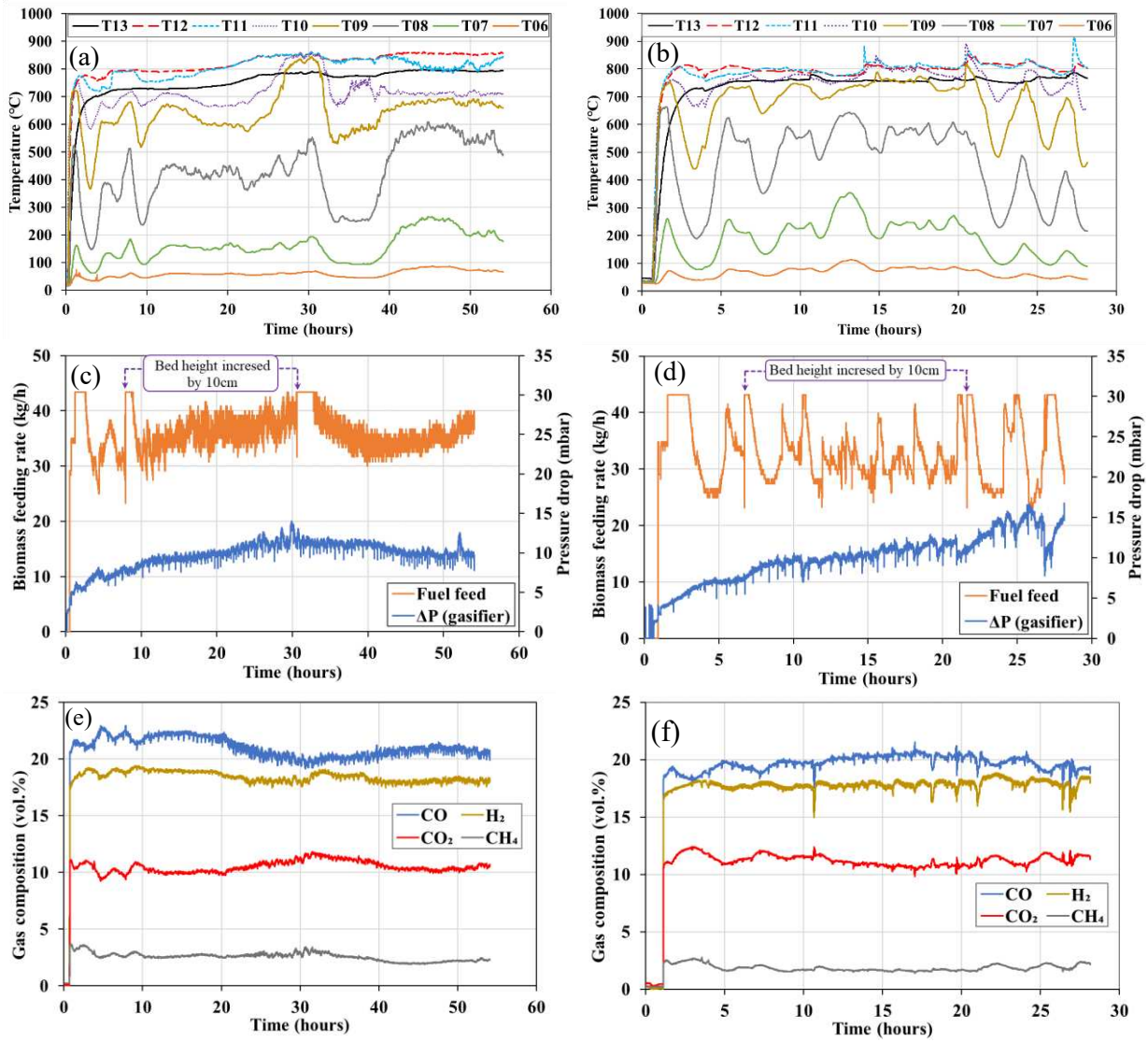


Fig. 4. Real-time measurements of (a, b) temperature distribution, (c, d) biomass feeding and pressure drop, and (e, f) gas composition at 65 kg/h air flow rate and 85-105 cm bed heights for wood pellets (left) and miscanthus pellets (right).

345 Between the 10th and 20th hour of operation, the gasifier performance was noticeably more
346 stable for both materials in terms of the temperature and consequently the gas composition. The
347 mean reactor top temperature (T12) was 800 °C for both materials. The composition of syngas
348 derived from wood pellets and miscanthus pellets exhibited more stable concentrations (lower
349 SDs) over these 10 hours of operation. The syngas composition generated from wood pellets had
350 much reduced variability during this operating time, as presented in Table 3. In the case of
351 miscanthus pellets, the variation in gas composition was a direct reflection of the bed condition
352 where there were fluctuations in biomass feeding rate and accordingly the temperature
353 distribution in the reactor vessel.

354 Table 3. Average and standard deviation of syngas composition during different time periods
355 of gasification at an air flow rate of 65 kg/h.

| Gas composition | CO | | $CO_2$ | | $CH_4$ | | $H_2$ | |
|---|---|---|---|---|---|---|---|---|
| | Mean | SD | Mean | SD | Mean | SD | Mean | SD |
| Time period: 1-10 hrs. of operation | | | | | | | | |
| Wood pellet | 21.80 | 0.49 | 10.28 | 0.46 | 2.90 | 0.31 | 18.86 | 0.30 |
| Miscanthus pellet | 19.25 | 0.47 | 11.57 | 0.40 | 1.98 | 0.33 | 17.74 | 0.22 |
| Time period: 10-20 hrs. of operation | | | | | | | | |
| Wood pellet | 22.10 | 0.18 | 10.06 | 0.13 | 2.62 | 0.09 | 18.94 | 0.10 |
| Miscanthus pellet | 20.21 | 0.38 | 10.95 | 0.35 | 1.67 | 0.09 | 17.81 | 0.33 |

356 In addition, it was noted that the biomass feeding rate varied over a larger range in the case
357 of the miscanthus pellets than wood pellets. This was attributed mainly to the formation of gas
358 channels or bridges inside the bed as a result of bed agglomeration. When these bridges
359 collapsed, the reactor experienced a sudden drop in the bed level, therefore the biomass feeding
360 rate surged to compensate for this change and achieve the set point of bed height, as can be
361 observed from Fig. 4d. The extent of these channels inside the bed increased over time because
362 of the ash sintering and incremental build-up of material into nodules. These were formed by the

363 molten inorganic metals in the miscanthus pellet ash agglomerating the material into increasingly
364 larger nodules that then combined to form the solid bridges. The fluctuation in biomass feeding
365 rate was often coincided with spikes in the gas composition, as seen in Fig. 4f, where the $H_2$ is
366 the species most affected, followed by the CO. Further, the collapse of the channels and bridges
367 formed caused a spike in the adjacent temperatures (mainly T11), often reaching approximately
368 900°C, as can be seen in Fig. 4b.

369 It is worth mentioning that the observed reduction in temperatures at T10-T7 at the 21$^{st}$ hour
370 during the gasification of miscanthus pellets owed to the intentional increase in the bed height
371 from 95 cm to 105 cm in an attempt to displace and/or break the nodules of sintered ash formed,
372 by introducing fresh biomass material.

373 In the case of wood pellets, the gasifier operated more consistently over a longer duration
374 compared to the miscanthus pellets, however, an unexpected excursion in the gasifier
375 temperature was noted after 20 hours of operation as seen in Fig. 4a. This was attributed to the
376 slow build-up of a stationary char agglomerate in the bed despite the low ash content in the wood
377 pellets compared to the miscanthus. This blockage caused de-fluidisation of part of the bed and
378 resulted in an increase in the localised gas velocity, which in turn increased the temperature (T8-
379 T10) [36]. Another indication of the existence of a blockage inside the bed was the increased
380 pressure drop through the gasifier which reached 13.5 mbar as demonstrated in Fig. 4c. The
381 temperature rise was an indication of combustion reactions being promoted and therefore the
382 $CO_2$ concentration increased at the expense of CO, as shown at the corresponding time in Fig.
383 4e. During this increase in the gasifier temperature, the CO concentration declined to a minimum
384 value of 19.6% while the $CO_2$ concentration increased to attain a maximum value of 11.6%.

385 The bed agglomerate was broken by increasing the bed height from 95 to 105 cm at the 31$^{st}$ hour,
386 which succeeded in returning the bed to a homogeneous fluidised condition.

387 The gasifier operation with wood pellets achieved a continuously operating duration of
388 approximately 54 hours without intervention, whereas the gasifier stopped after 28 hrs of
389 continuous operation for the miscanthus feedstock, due to the excessive buildup of slag in the
390 bed. The buildup of slag from miscanthus can be observed by the increase in the pressure drop
391 over the reactor as shown in Fig. 4d, where the pressure increased to approximately 17 mbar
392 within a shorter period of time compared to wood pellets.

393 It is worth mentioning that the biomass consumption rate of miscanthus pellets was lower than
394 that of the wood pellets despite having a similar calorific value (see Table 1). This difference in
395 material consumption rate was attributed to the tendency of the partly-gasified wood char
396 particles to leave the gasifier reactor along with the syngas, whereas in the case of miscanthus,
397 the ash sintering helped to retain the char particles in the reactor for longer durations, thus leading
398 to less of the solid material leaving with the syngas. This is supported by the proximate, ultimate,
399 and calorific value analyses conducted on the ash collected in the gas filter as depicted in Fig. 5
400 and Fig. 6. While the volatile matter was almost the same for both samples, the fixed carbon in
401 ash obtained from miscanthus gasification is lower than that obtained from wood pellet
402 gasification (66.2% vs 84.0%). In addition, the ash concentration in the sample of miscanthus is
403 more than double the corresponding concentration of ash from wood pellet gasification (30.1%
404 vs 12.3%).

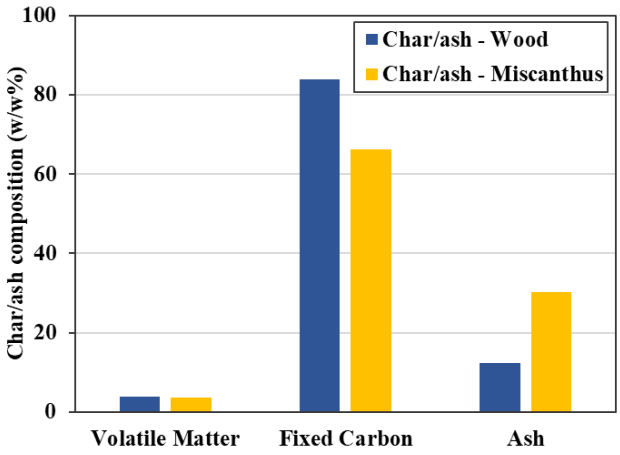


Fig. 5. Proximate analysis of the ash collected in the gas filter during the gasification of wood pellets and miscanthus pellets.

Further, the ultimate analysis indicates that carbon is the main element in both samples of ash with small traces of the other elements (H, N, O) as shown in Fig. 6. In this analysis, carbon represents 85.9% and 61.8% of the ash collected from the gasification of wood pellets and miscanthus pellets, respectively. Another major indicator of the extent of the energy conversion of solid fuel into syngas is the LHV of the by-product ash collected in the gas filter. The LHV of the two ash types was estimated using a bomb calorimeter, giving 21.1 MJ/kg and 28.5 MJ/kg for the miscanthus-based and wood-based ashes, respectively

This lower residual calorific value of the miscanthus ash than wood pellet ash suggests a higher conversion of the biomass calorific content to syngas, which explains the lower biomass consumption in the case of miscanthus pellet gasification compared to wood pellets.

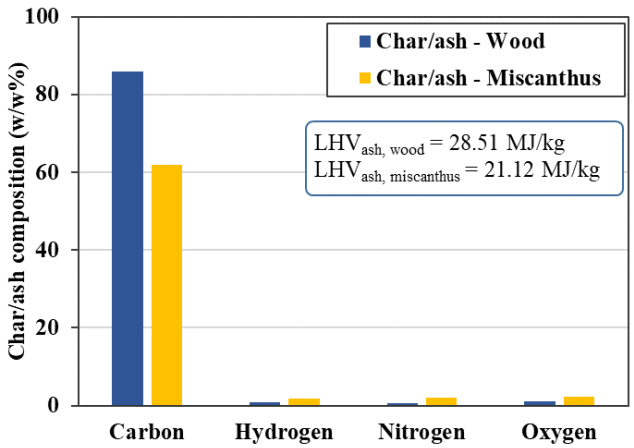


Fig. 6. Ultimate analysis and LHV of the ash collected in the gas filter during the gasification of wood pellets and miscanthus pellets.

## 3.2 Effect of air flow rate

### 3.2.1 Effect of air flow rate on bed condition

The effect of changing the air flow rate on the gasifier bed condition has been investigated because bed fluidisation is known to improve the gas-solid interaction [8] where air flow is its main driving force. The gasifier bed performed as expected while gasifying the wood pellet feedstock, where the bed fluidisation intensity changed according to the air flow rate with no noticeable locations of dead (static) regions within the reactor. This is attributed to the characteristics of wood pellets as a low-ash feedstock, thereby deterring agglomeration. Conversely, challenges for maintaining a homogeneous fluidisation state of the bed have emerged while gasifying miscanthus pellets which have higher ash content. Fig. 7 illustrates how the bed appeared at different air flow rates and at different operation times.

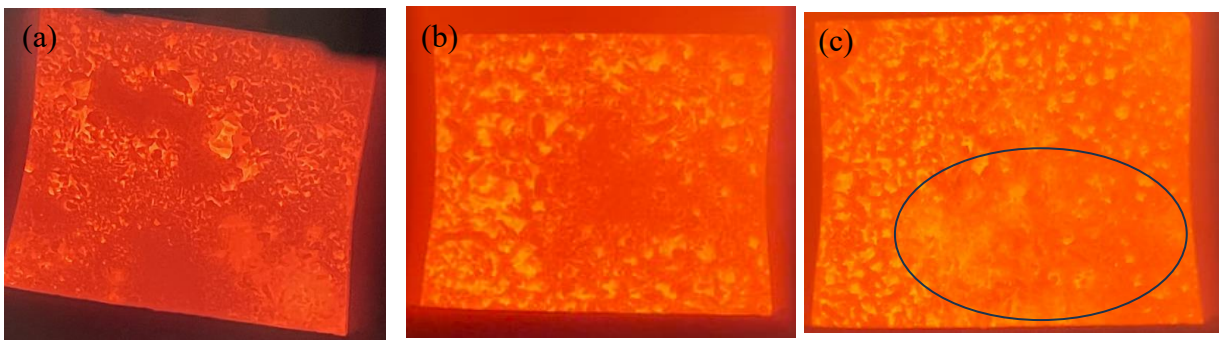

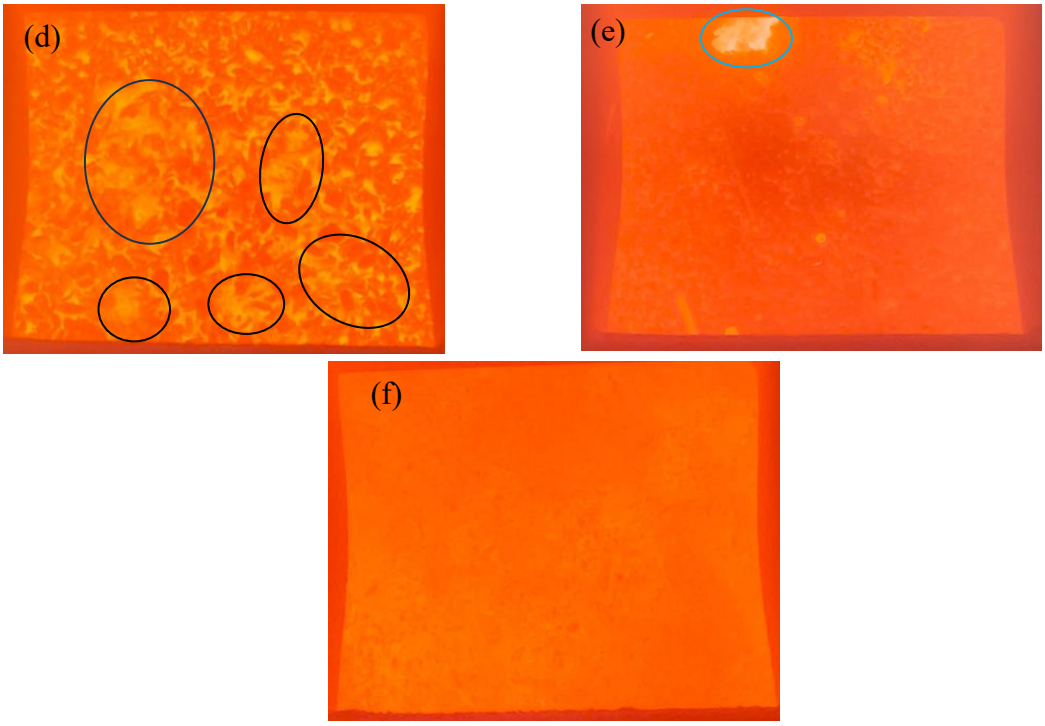


Fig. 7. Images of the top of the miscanthus bed with an air flow rate of 55 kg/h (a, b, c), 65 kg/h (d, e), and 75 kg/h (f).

For instance, Fig. 7a, b, and c show the bed conditions at a constant air flow rate of 55 kg/h over time. Fig. 7a shows the bed approximately 1.5 hours after start-up, and it is completely stationary (no sign of movement) whilst the reactor stabilised the bed height and achieved equilibrium between fuel feed rate and consumption for gas conversion. Fig. 7b demonstrates the bed condition with higher intensity radiation associated with initial stages of fluidisation, after approximately ~5.6 hours continuous operation. An area of fluidisation was observed in the bed after 7 hours of operation, highlighted by the black oval marked in Fig. 7c. It can be concluded that the longer the operation time after start-up and upon achieving steadier state operation at nominal continuous conditions, the more likely it was that the reactor achieved steady-state fluidisation. This is because the walls work as a heat sink and take a long time to reach stability. As the walls reach steady state temperature, the heat then available helps in promoting the pyrolysis of the particles into light char, which then become easier to fluidise [37]. However, this is not absolute as the extent of agglomerated ash, if any existed, grows over time in the reactor bed.

448 For the case of miscanthus gasification at an air flow rate of 65 kg/h, unlike the 55 kg/h case, the
449 bed is not stationary. After 2.5 hours of operation, portions of biomass are fluidised at the centre
450 and the lower side of the bed image shown in Fig. 7d. After a longer time of operation (26.5
451 hours) at 65 kg/h of airflow rate, the agglomeration of biomass ash and char has spread
452 throughout the top of the bed as illustrated in Fig. 7e, while most of the air is flowing through a
453 channel highlighted with the light blue oval. This slag buildup resulted in an increase in the
454 pressure drop to reach approximately 17 mbar across the reactor bed, as shown in Fig. 4d.

455 The effect of air flow rate on the bed condition becomes clearer when 75 kg/h airflow rate is
456 applied, where the fluidisation of the bed had become uniform and steady-state throughout the
457 cross-sectional area as illustrated in Fig. 7f, taken approximately after 5.5 hours of operation.
458 The bed appeared to have higher luminosity compared to the other images and was observed to
459 have many small perturbations of the surface. This fluidisation reduces the chances of
460 agglomeration build-up and helps in maintaining the gasification process for a longer time
461 between outages while also promoting a better interaction between the solid and gas materials.

462 It is worth highlighting that the homogeneity of the bed fluidity would be affected by scaling up
463 the gasifier as the diameter increases. The scale of the gasifier in this study is 200 $kW_{th}$, a pilot-
464 scale unit, and the bed condition should be further investigated for larger scales. Nevertheless,
465 the design of the gasifier allows for scaling up by modularity when reaching the limits of
466 maintaining homogeneous fluidisation in the reactor bed.

467 To illustrate the effect of bed condition on the gasifier performance in more detail, Fig. 8 depicts
468 the temperature distribution of the gasifier and the syngas composition from the gasification of
469 miscanthus pellets at a low airflow rate of 55 kg/h. The gasifier operated normally from the start-
470 up until about 9.5 hours had passed, where it reached a steady state gasification temperature of
471 approximately 750 °C through much of the bed depth, which was a relatively lower mean
472 temperature than measured for the other cases at higher airflow rates. This is because of the

reduction in heat release rate from combustion reactions in the gasifier when it is operated at low power (i.e., low air flow and low fuel feed rates). During this period, the syngas reached a steady state composition after about 5 hours, where the CO gradually increased from 18.6% to 20.0%, the $CO_2$ decreased from 12.2% to 10.8%, and the $CH_4$ decreased from 3.0% to 2.2%. Interestingly, the change in $H_2$ content was relatively small and the average concentration was 18.2 % as seen from Fig. 8b.

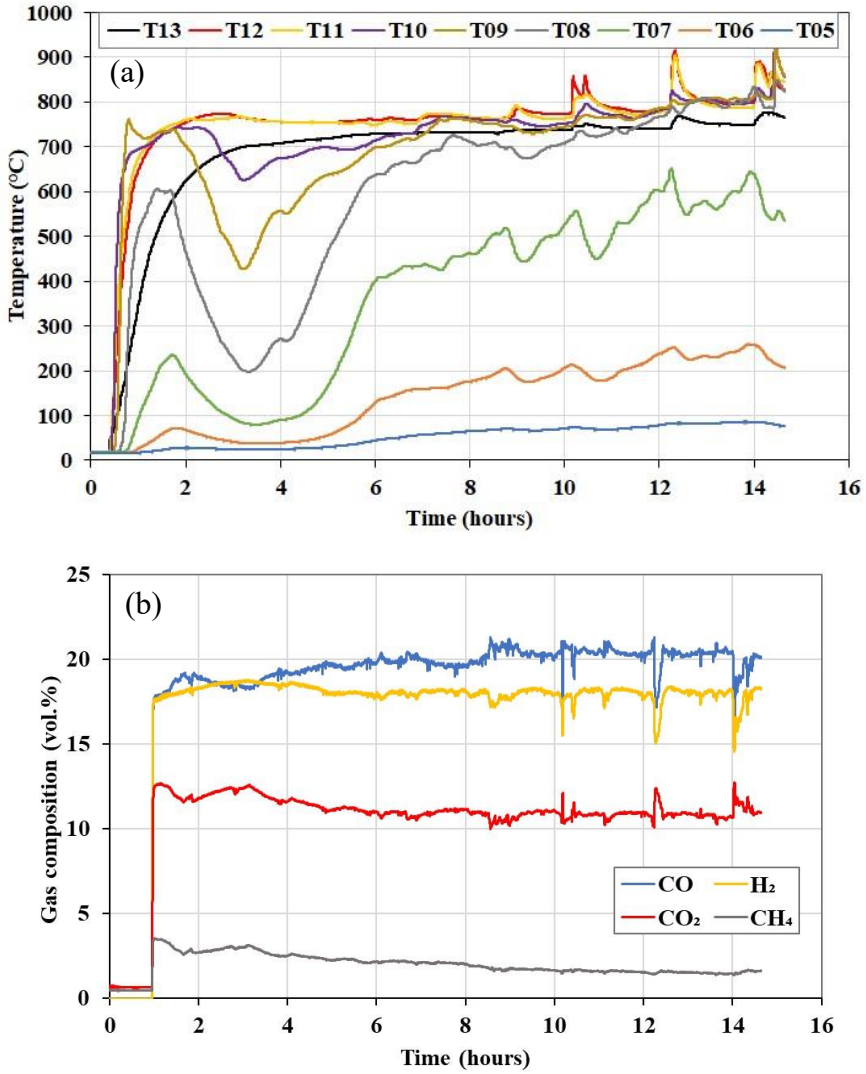


Fig. 8. (a) Temperature distribution and (b) syngas composition for the gasification of miscanthus pellets at an air flow rate of 55 kg/h.

Further, at around the 9.5-hour mark of operation, the formation of slag and channels in the bed had become effective to the extent of creating temperature spikes, indicating the formation followed by the collapse of bridges within the reactor bed. This behaviour occurred three times

484 within 4 hours of operation, which led to the shutdown of the gasifier by the control system. This
485 build-up and collapse of agglomerated material bridges is mainly because of the absence of bed
486 fluidisation at this low air flow rate, where the bed was noticed to be mostly stationary, especially
487 in the early hours of operation while the gasifier reactor was being warmed up. This confirms
488 that sufficient fluidisation is essential to mitigate the effect of slag formation.

489 **3.2.2 Effect of air flow rate on gas species (FTIR analysis)**

490 The characterisation of the syngas produced was extended further to account for the changes
491 in different hydrocarbon compounds, nitrogen-based compounds and water vapor content under
492 different operating conditions. It is important to mention that the aforementioned gas analysis
493 discussed at the start of Section 3.1, is based on the online gas analyser which measures all
494 hydrocarbon compounds and reports these to be methane, which is the principal hydrocarbon
495 species formed and presented as analysis on a dry basis. Analysis of the gasifier product gas
496 using FTIR spectroscopy was essential to achieve a more comprehensive understanding of the
497 species generated and to assess the gasifier performance. Total Organic Carbon (TOC)
498 measurement in the syngas is helpful to quantify the "cleanliness" and energy density of the
499 syngas produced. In this context, TOC represents the organic compounds that haven't been fully
500 cracked into permanent gases (CO, $H_2$, $CO_2$, and $CH_4$). Since tars are organic carbon, a TOC
501 measurement acts as a proxy for tar concentration. TOC also helps in presenting the carbon
502 conversion efficiency of the gasification process. Fig. 9 depicts the changes measured in TOC
503 with a representation of the changes in methane and other hydrocarbon compounds when the
504 supplied air flow rate is increased from 50 to 75 kg/h while gasifying wood pellets. Most of the
505 results in this section are based on wood pellets as it gives more stable results than in the case of
506 miscanthus which encountered issues with bed fluidisation stability.

507 The concentrations of TOC, $CH_4$ and other hydrocarbon compounds reduced with increasing
508 air flow rate, indicating an improved syngas quality achieved by the conversion of tars (heavy

hydrocarbons) to lighter gases, mainly CO and $CO_2$. For instance, the TOC reduces from 10.6 g/m$^3$ at 50 kg/h to 6.1 g/m$^3$ at 75 kg/h air flow rate, representing a reduction in TOC by 42%. Since $CH_4$ represents the major compound of TOC, the concentration of $CH_4$ reflects these changes as it reduces by 37% as shown in Fig. 9.

Other hydrocarbons including $C_2H_2$, $C_2H_4$, $C_2H_6$, $C_4H_6$, and $C_9H_{12}$, were reduced to low levels, concurrently with the reduction of the methane concentration. The concentration of $C_2H_4$, $C_2H_2$, and $C_4H_6$ exhibited significant reductions of 76%, 89%, and 84%, respectively when the air flow rate was increased from 50 to 75 kg/h. The other hydrocarbon compounds were reduced to concentrations of circa 50 ppm which may be considered to be negligible

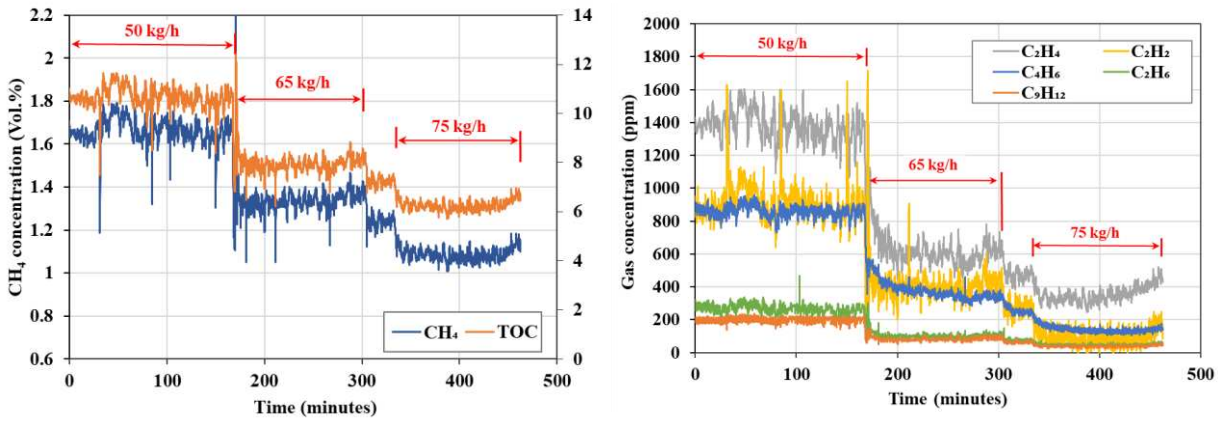


Fig. 9. TOC content and concentrations of hydrocarbon compounds in the wet syngas from wood pellets gasification at different air flow rates.

This reduction of TOC is mainly attributed to the increased gasification temperature inside the gasifier as a result of increasing the air flow rate, which helps in thermally cracking the tar compounds [38]. This high temperature, in particular when accompanied by the presence of steam, in this instance sourced from inherent biomass moisture (7.4 wt.% in the initial wood pellets), enhances the steam reforming and secondary cracking reactions of the tar to produce lighter gases, including some hydrogen and CO through enabling subsequent (Boudouard) reactions [38]. This reduces tar concentrations in the syngas, therefore improving overall syngas quality. This can be observed by the slight reduction in water vapor concentration in the wet

syngas from 10.8% to 9.6% when the air flow rate increases from 50 to 75 kg/h as shown in Fig. 10. It is worth noting that the water vapour and $NH_3$ peaks noticed in Fig. 10 are attributed to the occasional condensation of water droplets. This is confirmed by the synchronised peaks of $H_2O$ and $NH_3$ as the Ammonia is highly hygroscopic, i.e. $NH_3$ dissolves incredibly well in water [39].

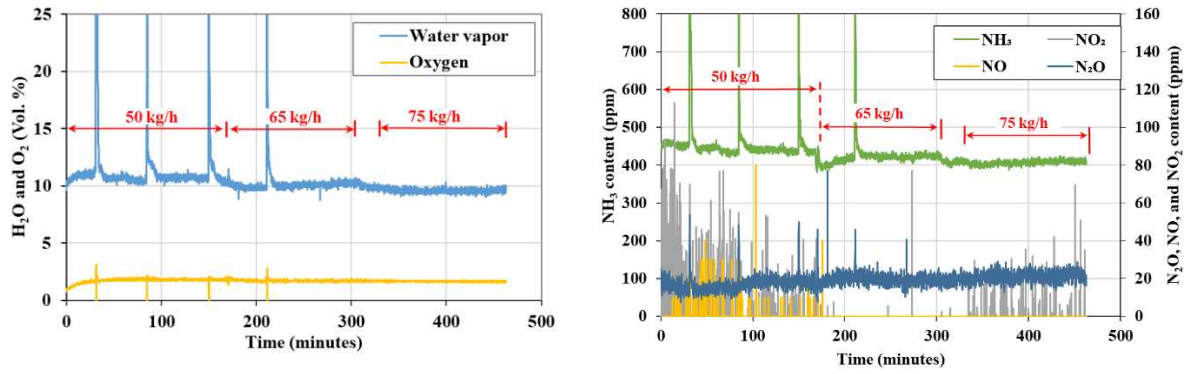


Fig. 10. Concentrations of water vapor, oxygen, and nitrogen-based compounds in the wet syngas from the gasification of wood pellets at different air flow rates.

To characterise the remaining compounds in the syngas, it is important to highlight that oxygen is almost constant regardless of the supplied air flow rate as illustrated in Fig. 10. This reflects that a consistent interaction between air and biomass is achieved as a result of the fluidity of the bed and the action of the control system.

The relationship between the air flow rate and the biomass consumption rate, and the corresponding ER while operating under the control of constant airflow, is shown in Fig. 14.

In addition, it is important to extend this analysis to include the nitrogen-based compounds that could be present in the syngas produced and what effects the operating conditions have on their generation and consumption. Fig. 10 shows that $NH_3$ was the major compound with a concentration of $\geq$ 400 ppm, where this concentration reduced slightly with the increase of air flow rate. Similarly to the effect of high temperature on boosting the tar reforming reactions, the ammonia content has been found to reduce under the high temperature of the gasification process, as a result of ammonia decomposition [38].

When it comes to the nitrogen-based oxides, N2O, NO, and NO2 are present at trace concentrations with values as low as 20 ppm as depicted in Fig. 10. The changes in NOx concentration and uncertainty around the mean magnitude observed for wood pellets were not replicated when feeding miscanthus pellets as can be observed from Fig. 11. The increased uncertainty around the mean NOx concentrations arising was attributed to the challenges of achieving stable operation with miscanthus pellets compared to wood pellets. It is worth noting that the extent of ammonia in the produced syngas form miscanthus is higher than that from wood pellets by more than 3 folds as can be seen in Fig. 10 and Fig. 11. This is attributed to the more nitrogen present in miscanthus compared to wood as shown in Table 1, where miscanthus has nitrogen content 3 times the content in wood pellets.

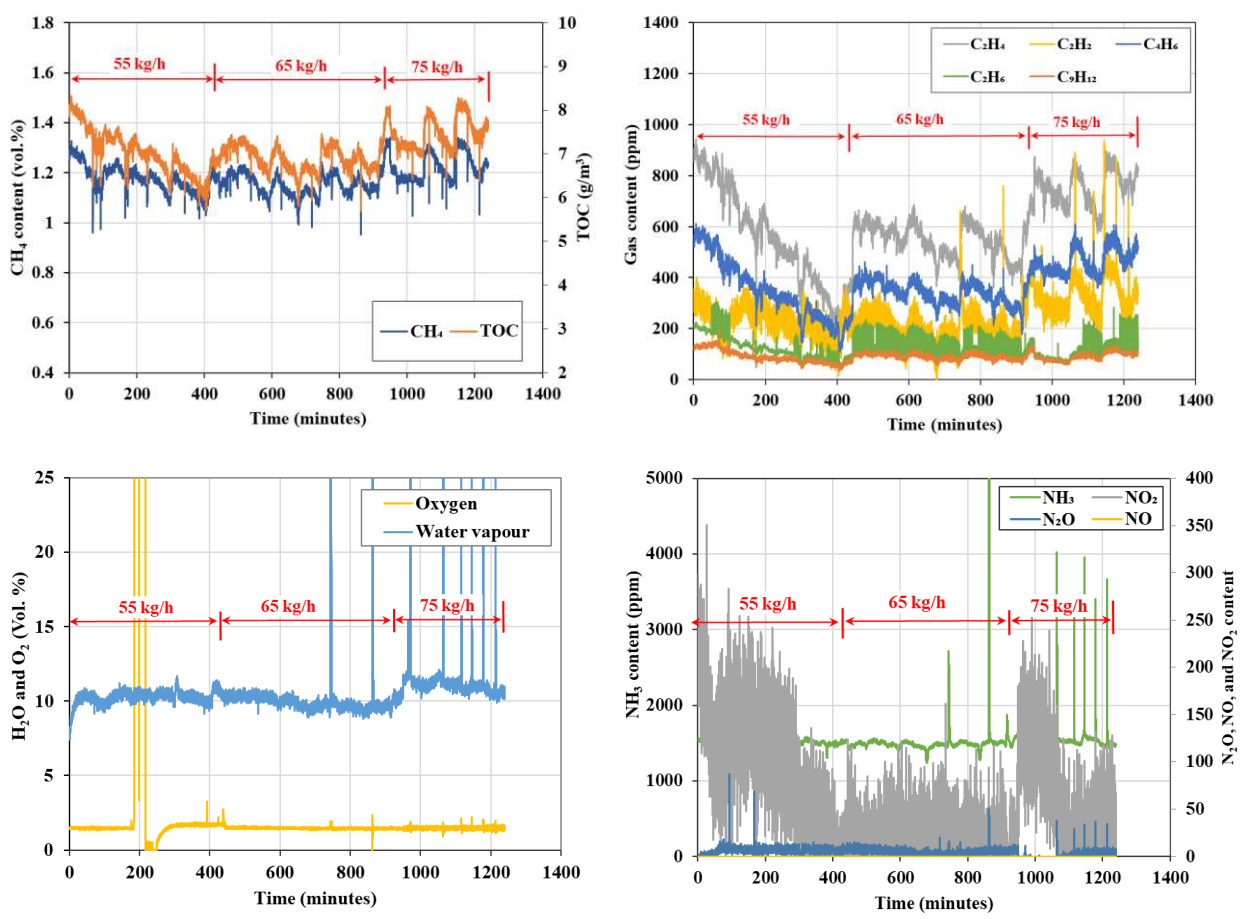


Fig. 11. Results of FTIR analysis of wet syngas from miscanthus pellets gasification at different air flow rates.

### 3.3 Effect of gasifier operating condition on tar content

The concentration of tar present in the syngas is critical for any biomass conversion process due to its detrimental effect on syngas applications, for example causing fouling of heat exchangers and reactor surfaces, catalyst degradation, and coking in high temperature plant.

As noted in the work of Barisano et al. [6] and Rey et al. [7], high levels of tar content may require further processing or removal to improve syngas quality, especially if the syngas is intended for applications like synthetic aviation fuel generation or as a feedstock for chemical synthesis.

Table 4 presents the estimated tar content in the syngas at different operating conditions, where the highest amount of 163.5 mg/Nm$^3$ was collected from the gasification of miscanthus pellets at 55 kg/h air flow rate and 85 cm bed height. In comparison, the highest tar content collected from syngas produced from wood pellets under the same conditions is significantly lower, at 54.2 mg/Nm$^3$. The high tar content in the syngas from miscanthus at low air flow rates is mainly attributed to the reactor bed condition, where there is no fluidisation, hence reducing the chances of tar cracking. The tar content was the lowest for miscanthus and wood pellet gasification at the higher air flow rate of 75 kg/h, producing tar concentrations of 63.0 and 14.7 mg/Nm$^3$, reductions of 61% and 73% respectively compared to the tar concentration in syngas generated at an airflow of 55 kg/h for the same bed height. This was due to the higher temperatures observed here and, along with the moisture present, the steam reforming and tar cracking reactions that were then able to occur. This range of tar contents emphasizes the vital impact of the reactor temperature on tar cracking, as previously mentioned in Section 3.2.1, along with the fluidization intensity of the bed, which is mainly governed by the air flow rate. This range of tar contents from the rising co-current gasifier makes it comparable to or even better than the downdraft gasifier [17]. To put this into perspective, tar content in the product gas from

585 the other types of fixed bed gasifiers is typically between 2 and 20 g/Nm$^3$ (dry basis) [40], and
586 the average tar content is in the range of 1-30 g/Nm$^3$ for fluidized bed gasifiers [41]. For instance,
587 Liu et al. [42], reported a tar concentration of 15.8 g/Nm$^3$ for fluidised bed gasification using
588 rice straw.

589 Table 4. Tar content in the syngas at different operating conditions.

| Air flow rate (kg/h) | Bed height (cm) | Wood pellets (mg/Nm$^3$) | Miscanthus pellets (mg/Nm$^3$) |
|---|---|---|---|
| 55 | 85 | 54.2 | 163.5 |
| 65 | 85 | 16.5 | 68.0 |
| 65 | 95 | 32.9 | 78.9 |
| 65 | 105 | 41.7 | 86.5 |
| 75 | 85 | 14.7 | 63.0 |

590 The effect of bed height on tar content was evaluated and demonstrated that the tar
591 concentration increased from 68.0 mg/Nm$^3$ to 86.5 mg/Nm$^3$ for miscanthus and from 16.5
592 mg/Nm$^3$ to 41.7 mg/Nm$^3$ for wood pellets, with increasing the bed height from 85 cm to 105 cm,
593 as presented in Table 4 The increased tar concentration can be attributed to the larger portion of
594 the bed that had been fluidised, where the formation of macroscopic scale bubbles occurred.
595 These larger bubbles reduced the total number of bubbles across the bed, thereby limiting the
596 solid-gas interactions necessary for effective tar reduction. Additionally, increasing the bed
597 height during operation expands the gasification zones, resulting in the heat being distributed
598 over a larger portion of the biomass. Given that the heat generation rate remains nearly constant
599 (due to the fixed airflow rate), the bed temperature decreases, leading to reduced tar cracking.
600 As demonstrated, the gasification of wood pellets produced higher-quality syngas with lower tar
601 content compared to miscanthus pellets. Also, higher bed temperatures and lower bed heights
602 resulted in better quality syngas from both feedstocks. However, tar content cannot be the only
603 criterion for selecting the gasifier operating conditions and feedstock, therefore, the efficiency
604 of converting biomass energy into syngas was evaluated.

### 3.4 Gasifier performance assessment

Gasifier performance was evaluated for the different operating conditions for both feedstocks. Given that gasification is an energy conversion process, the syngas LHV, CGE and CCE were investigated based on the average gas composition shown in Fig. 12 and Fig. 13. It is worth highlighting that the average gas composition from wood pellets at 65 kg/h was replaced by results from another test run where the gasifier was running under the control of the CHP unit at an average air flow rate of 66.6 kg/h. This data set is presented in the supplementary material, and it was selected for this figure due to the stability of syngas composition for a long time.

Fig. 12 depicts that both CO and $CO_2$ concentrations in the syngas tend to behave opposite to each other during the gasification of both feedstocks when the supplied air flow rate is changed. Similar behaviour was observed by Guo et al. [32]. This is expected for a steady-state operation of the gasifier, where both CO and $CO_2$ are the main components representing the carbon conversion from biomass to the gas phase. Hence, the extent of each species in the syngas should be balanced by the change of the other species to maintain the mass balance of carbon. Regarding the effect of the biomass feedstocks on the changes in gas composition, the CO concentration increased from 20.3% to 21.9% (+8.0%) as the airflow increased during wood pellet gasification, while it slightly decreased from 20.1% to 19.6 (-2.7%) during the gasification of miscanthus pellets. This can be ascribed to the condition of the gasifier bed, particularly the extent of fluidisation. As discussed earlier, a larger amount of pyrolysed carbon (char) tends to leave the gasifier and travel out with the syngas, which increased the supply rate of fresh biomass during the gasification of wood pellets compared to miscanthus. This boosts the contribution of biomass decomposition products (pyrolysis syngas) to the final syngas composition by increasing the CO content in the case of wood pellets. This effect is also observed during miscanthus pellet gasification at the maximum air flow rate of 75 kg/h, where the CO concentration starts to rise as shown in Fig. 12. In addition, as previously noted in Section 3.1, the miscanthus pellets had

higher moisture content and lower VM and carbon content than the wood pellets which favoured the production of $CO_2$ over CO.

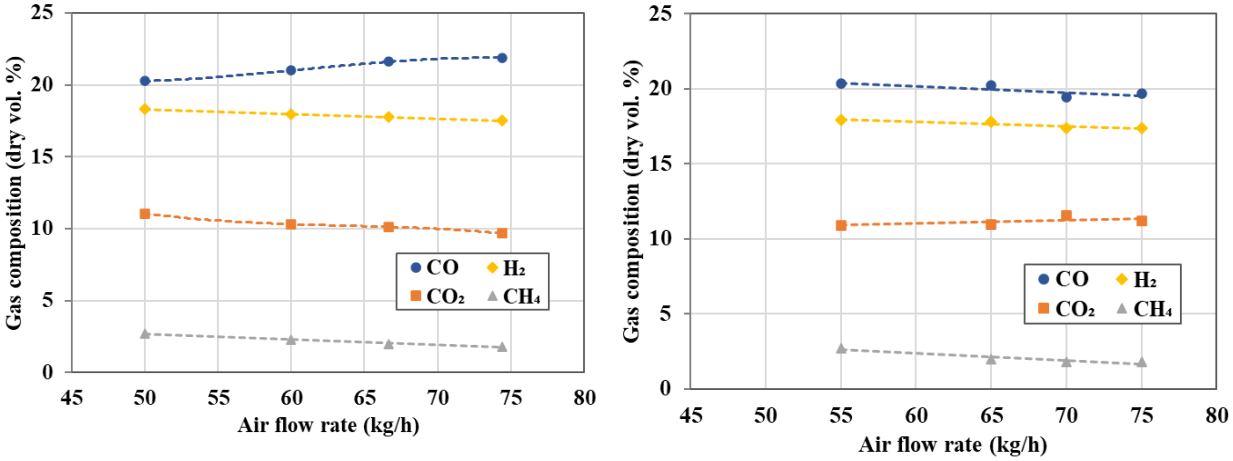


Fig. 12. Average gas composition of syngas from wood pellets (left) and miscanthus pellets (right) at different air flow rates.

The other components of syngas tended to decrease during the gasification of both feedstocks when the airflow rate was increased. While $H_2$ content in the syngas derived from wood pellets incurred a slight reduction from 18.3% to 17.5%, potentially due to additional dilution, a more noticeable change in the $CH_4$ content from 2.7% to 1.8% was observed when the airflow rate increased from 50 to 75 kg/h as illustrated in Fig. 12. Similarly, the $H_2$ content from miscanthus pellets reduced from 17.9% to 17.4%, and $CH_4$ reduced from 2.8% to 1.8% when the air flow rate increased from 55 to 75 kg/h. Nevertheless, the $H_2$ content from both feedstocks was higher than reported in a number of different studies of different gasifier designs. For the wood pellets case, the average reported $H_2$ content is in the range 12.7 – 16.5% using BFB gasifiers [12, 13]. In case of miscanthus, the study of Khan et al., reported a H2 content of 5.1% from a downdraft gasifier [21].

The reduction in $CH_4$ is attributed to the reduction in residence time as the air flow rate increased, which in turn affected the slow reactions, such as the hydrogasification reaction, which contributes to the formation of $CH_4$ [5, 43]. Additionally, the increase in gasifier temperature boosts the tar cracking reactions and results in a reduction in the hydrocarbon compounds.

649 The syngas LHV and gasifier energy and mass conversion efficiencies were evaluated to
650 assess the process performance in terms of biomass input to gas output conversion. Fig. 13
651 reveals the LHV of syngas, the CGE and CCE of the process for both feedstocks under different
652 air flow rates. It is evident that the syngas produced from wood pellets had a marginally higher
653 LHV compared to that produced from miscanthus pellets, particularly at the high air flow rates.
654 This suggests that wood pellets are more effective in generating energy-rich syngas. However,
655 the LHV of syngas from both feedstocks decreased when the airflow rate increased. For instance,
656 as the airflow rate increased from 50 to 75 kg/h during the gasification of wood pellets, a gradual
657 decline in the average syngas LHV from 5.5 MJ/Nm$^3$ to 5.3 MJ/Nm$^3$ was observed. Also, a
658 similar reduction occurs in the LHV of syngas from miscanthus pellets, which reduced from 5.4
659 MJ/Nm$^3$ to 5.0 MJ/Nm$^3$. The decrease in LHV can be attributed to the reduction within the
660 syngas composition of the $H_2$ and $CH_4$ concentrations, which have calorific values significantly
661 higher than that of CO. Another major factor that controls the LHV is the dilution effect, where
662 the increased introduction of air into the gasifier results in more nitrogen being mixed with the
663 syngas, thereby reducing its overall calorific value [32]. It is worth mentioning that the syngas
664 LHV is higher than that of syngas produce from woody biomass using fixed bed reactor (3.8-4.8
665 MJ/Nm$^3$) [14-17] and using fluidised bed gasifiers (5.6 MJ/Nm$^3$) [13]. Although the LHV of the
666 syngas in this study is lower than that reported in the study of Pio et al. [12] from a BFB gasifier,
667 the co-current gasifier CGE and CCE calculated were higher. The CGE of the gasification of
668 wood pellets in the co-current gasifier was estimated to lie in the range 77-83% whereas it lied
669 in the range 50-57 for the gasification of wood pellets in the BFB gasifier. For the CCE, the co-
670 current gasifier shows values in the range 88-93% vs 70-80% for the BFB gasifier [12].

671 Also, the LHV of the syngas from miscanthus is still better than that derived by gasification
672 of miscanthus in a downdraft gasifier, where the HHV was reported as 4.2 MJ/Nm$^3$ [21].

673 The quality of syngas produced from this gasifier at this scale (200 $kW_{th}$) in terms of tar
674 content and LHV makes it perfect for many applications, such as combined heat and power
675 generation applications (CHP) for decentralised energy systems. Furthermore, it would be a
676 valuable option for biofuels production with the potential of scaling up through modularity.

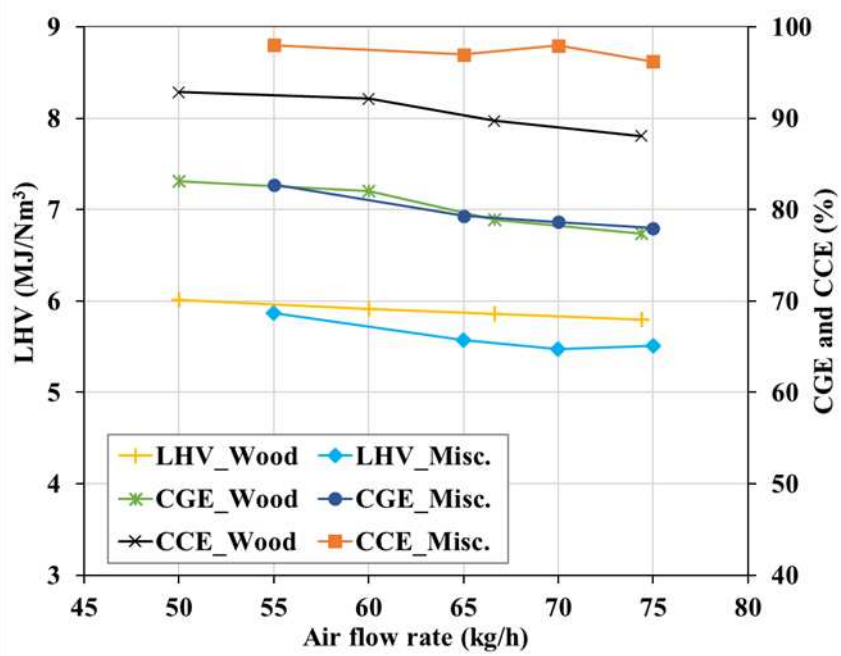


677

678 Fig. 13. Effect of air flow rate on the LHV of syngas and CGE and CCE of the biomass
679 gasification process of wood pellets and miscanthus pellets.

680 Although the LHV is a significant parameter for assessing syngas quality, alone it is insufficient
681 to fully evaluate the biomass conversion process. Therefore, CCE is critical because it indicates
682 the extent to which biomass (in terms of carbon) is converted into syngas, which directly impacts
683 the fuel consumption rate. Fig. 13 illustrates that despite the relatively higher LHV of syngas
684 produced from wood pellets, the CCE for miscanthus pellets exceeded that of wood pellets across
685 all tested airflow rates. The CCE for miscanthus remained relatively constant, ranging between
686 96.2% and 98.0%, whereas for wood pellets, it declined from 92.9% to 88.0% as the airflow rate
687 increased. This trend was primarily attributed to the effects of intensified bed fluidisation at
688 higher air flow rates, where substantial amounts of pyrolyzed char are carried out of the gasifier

reactor by the syngas. This phenomenon was more pronounced in the gasification of wood pellets, as previously discussed in Section 3.1.

Furthermore, it was even more evident when examining the relationship between the air flow rate and the biomass consumption rate for both fuels as shown in Fig. 14. It can be seen that both feedstocks exhibited a linear relationship between the air flow rate and the biomass consumption, however these trends diverged with increased air flow rates. The relationship indicated a higher expulsion rate of char/ash particles in the case of wood pellets compared to miscanthus pellets. The high expulsion rate of char/ash incurs high consumption rate of biomass, and this explains the steeper slope in the case of wood pellets compared to miscanthus pellets.

The linear relationships between air and biomass consumption were reflected in the estimated Equivalence Ratio (ER), which remained nearly constant at 0.283-0.287 during the gasification of wood pellets at different air flow rates. In the case of miscanthus pellets gasification, ER increased from 0.319 to 0.339 when the air flow rate increased from 55 kg/h to 75 kg/h. The estimated values of ER lie in the range 0.2-0.37, which is reported as the operable range for wood pellets and miscanthus pellets gasification [44].

It can be concluded that biomass type determines the operating ER when using the same gasifier reactor. A similar conclusion was reached by Meng et al. for corn stalk and pine wood feedstocks [45]. However, the estimated ER for gasifying wood pellets in the current study is lower by 0.04 than that reported for wood in their study (0.33) [45] and higher by 0.04 than the optimum ER with maximum $H_2$ content in the syngas from the BFB gasifier (0.24) [12]. Similarly, the estimated ER for the gasification of miscanthus pellets is higher than the ER of gasifying miscanthus pellets in a downdraft gasifier (0.28) in the study of Kallis et al., [24]. This is due to the high conversion rate of miscanthus pellets in the current study.

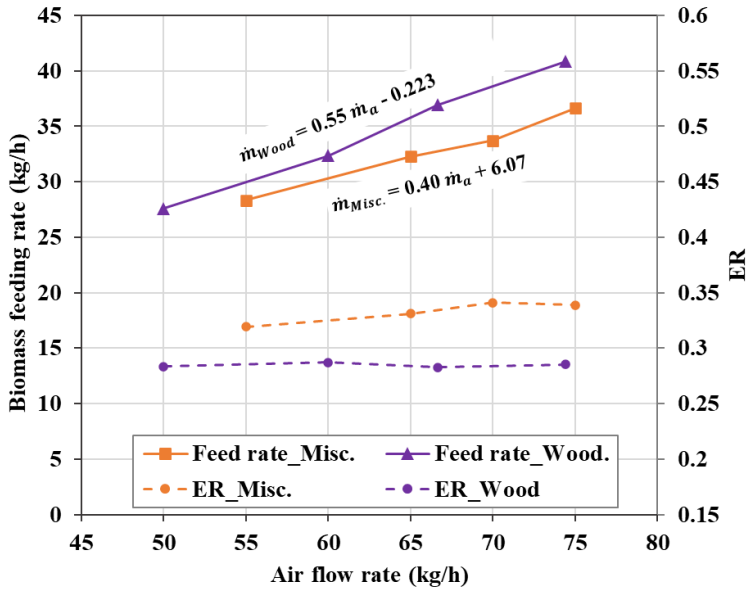


Fig. 14. Effect of air flow rate on the consumption rate of wood and miscanthus pellets and the ER.

The combined effect of the changes in syngas LHV and CCE was mirrored in the trend of the estimated CGE as illustrated in Fig. 13, where both feedstocks exhibited similar trends across the air flow rates investigated. The CGE was estimated to range from 77.3% to 83.1% for both feedstocks, which is much higher than the values reported in the literature. For instance, the CGE was estimated as 30% in the study of Kallis et al. [24], 58% in the study of Couto et al., [20], and 62% in the study of Xue et al [23].

This highlights the compromises in determining operational conditions, where higher air flow might enhance certain aspects of the process, such as fluidization and tar content but at the cost of reduced syngas LHV and conversion efficiency. Thus, depending on the syngas application, for example, power generation or production of biofuels and/or $H_2$, the optimum operating conditions appropriate to the final product should be determined and applied.

### 3.5 Analysis of biomass ash and slag

In order to characterise the ash content of the biomass ash and the slag formed in the bed, ICP-OES and XRF analyses have been conducted on 3 samples collected from operating at different conditions. The composition of the chemical elements in the slag and biomass ash are

730 presented in Fig. 15 and Fig. 16, respectively. . It can be seen that the silicon (Si) and calcium
731 (Ca) content in the miscanthus was higher in the slag compared to the biomass ash. This is
732 potentially because most of the calcium binds with silica to form stable compounds, such as
733 wollastonite ($CaSiO_3$) in the reactor bed [46], whereupon it was retained, which lowers the
734 amount of calcium in the biomass ash.

735 Analysis of the Si content arising from wood pellets demonstrated the same trend of having a
736 higher amount remaining in the slag compared to the biomass ash. Ca and Mg were observed in
737 wood pellet char, ash and slag, which indicated contributions from heterogeneous condensation,
738 agglomeration and coalescence. This significantly influences the compositions of the biomass
739 ash particles generated during the gasifier operation [47]. The presence of Ca and Mg indicates
740 that these elements acted as a molten binder, condensing onto particle surfaces and causing them
741 to fuse together. Conversely, the potassium level is higher in the biomass ash compared to the
742 slag from both feedstocks. This is inferred to be due to potassium being a highly volatile metal
743 at high temperatures that can exist in the aerosol phase at the gasification temperatures incurred,
744 enabling its transfer with the syngas to the bag filter. In addition, the chlorine/chloride content
745 in wood pellets was low, representing 0.05 wt.% of the fuel composition (see Table 1), and it can
746 be assumed that the majority of the K released during gasification arose from the evaporation of
747 KOH. This compound has a lower melting temperature, 405 °C compared to KCl, hence the
748 KOH exhibits a higher degree of mobility in the gasification process.

749 According to Clery et al. [48] the evaporation of KOH will compete with the reaction mechanism
750 to fix the potassium in the ash (e.g. potassium aluminium silicate formation) and this could
751 explain the high mobility of potassium into the syngas that carried the biomass ash. It is important
752 to mention that the K released should be minimized to avoid the fouling problem on surfaces
753 because it can be in the form of KOH and/or KCl depending on the water content [49]. The
754 formation of KCl and KOH can be expressed as follows [50]:

$$2KO + H_2O \rightarrow 2KOH$$

$$KO + HCl \rightarrow KCl + OH$$

There was an increase of about 1.5 times in the phosphorus from 3.3 wt.% to 8.2 wt.% in the slag formed from miscanthus compared to wood pellets. This probably arose due to the formation of alkali phosphates in the slag that can pose several challenges to gasifier operations by forming KOH or phosphoric acid, both of which will cause corrosion of the reactor. There were no significant changes in Na and Al in the chemical element distributions in slag and biomass ash from either feedstock.

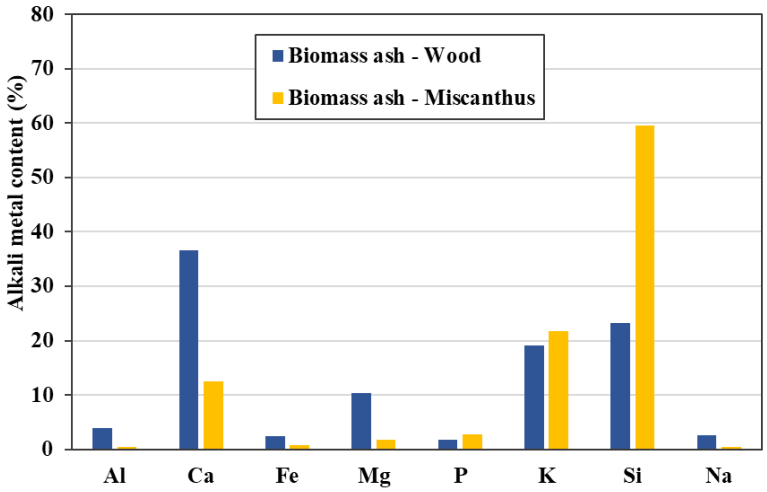


Fig. 15. The elemental content (normalised to 100%) in the biomass ash released from the gasifier.

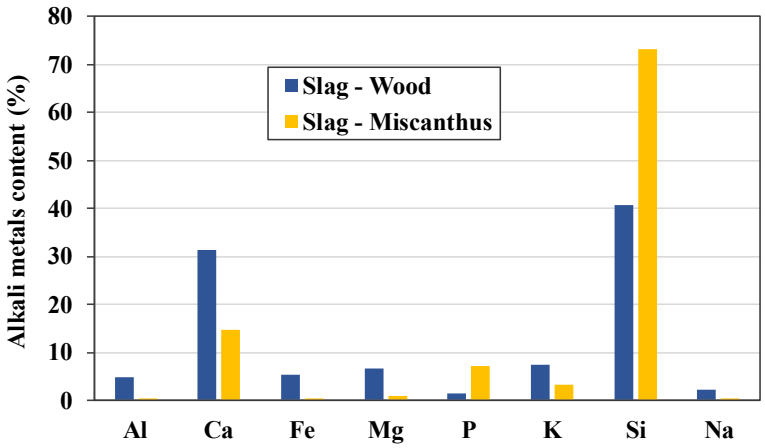


Fig. 16. The elemental content (normalised to 100%) in the slag from the reactor bed.

## 4 Conclusion

The novel design of the rising co-current gasifier shows excellent potential for producing high-quality syngas (high LHV with minimum tar content in the unrefined syngas generated), whilst maintaining acceptable material conversion efficiency. This study presented a comprehensive characterization of the rising co-current gasifier demonstrating its capabilities and limitations, across a range of operating conditions.

- The syngas produced from both wood and miscanthus pellets has an LHV in the range of 5.0-5.5 MJ/$Nm^3$, which is suitable for CHP applications and biofuel production. With this high LHV, the system has maintained a very low tar content (as low as 14.7 mg/$Nm^3$ from wood pellets and 63 mg/$Nm^3$ from miscanthus pellets) compared to other conventional fluidized bed configurations and updraft gasifiers.
- The operable range of ER for gasification varies with biomass feedstock; for wood pellets, a nearly constant ER at 0.283-0.287 was estimated at different airflow rates, whereas a higher ER was estimated for miscanthus pellets gasification at 0.319, slightly increasing to 0.339 with airflow rate.
- The $H_2$ concentration in the syngas was estimated to be as high as 18%, outperforming other types of gasifiers for generating hydrogen-rich syngas.
- Increasing the air flow rate reduced the LHV slightly but enhanced the fluidization of the bed and consequently reduced the tar content. However, the higher the air flow rate is, the lower the CCE becomes because of the increased carry over of the biomass char/ash.
- High CGE in the range of 77.3-83.1% was attained during the gasification of wood and miscanthus at different operating conditions. Furthermore, the CCE of wood pellets was estimated to lie in the range of 88.0-92.9%, whereas ultra-high CCE values (96.2-98.0%) were attained during the gasification of miscanthus.

- The relatively lower CCE of wood pellets led to the calorific value of the biomass ash being higher than the CV of biomass ash from the miscanthus pellets because more of the unreacted carbon had passed into the gases as solid char particles. The LHV of wood pellet biomass ash was 28.5 MJ/kg compared to 21.1 MJ/kg for the miscanthus-based biomass ash.
- Biomass with high ash content, such as miscanthus, can be gasified in the rising co-current gasifier, but fluidization of the bed is essential to mitigate slag formation and eliminate channelling problems caused by material agglomeration and slag formation that obstruct the gas flow path.
- Si, P and Ca were the major metallic and semi-metallic compounds retained from the biomass in the slag, while most of the K was inferred to have left the gasifier with the syngas and biomass ash, likely due to its volatility.

This information is critical for optimising gasification processes, particularly in selecting appropriate feedstocks and operational settings to achieve the desired compromise between material conversion efficiency and syngas quality. Achieving optimal operating conditions is crucial for syngas applications such as power generation or as a precursor for synthetic fuels.

**Acknowledgments**

The first author acknowledges The Egyptian Ministry of Higher Education & Scientific Research and The British Council (Newton-Mosharafa Fund) for funding this research study at the University of Sheffield. Also, the authors acknowledge that the EIC Facilities, part-funded by the European Regional Development Fund, were used for the experimental work reported herein. The research was financially supported by UKRI Industrial Decarbonisation Research and Innovation Centre (IDRIC) under the project number MIP 8.3 SAF production from biomass gasification.

816

# References


1. Committee, C.C., *Progress in reducing emissions—2023 report to Parliament. Jun 2023*.
2. Di Blasi, C., G. Signorelli, and G. Portoricco, *Countercurrent fixed-bed gasification of biomass at laboratory scale.* Industrial & Engineering Chemistry Research, 1999. **38**(7): p. 2571–2581.
3. Nguyen-Thi, T.X., et al., *Recent advances in hydrogen production from biomass waste with a focus on pyrolysis and gasification.* International Journal of Hydrogen Energy, 2023.
4. Heidenreich, S. and P.U. Foscolo, *New concepts in biomass gasification.* Progress in Energy and Combustion Science, 2015. **46**: p. 72–95.
5. Basu, P., *Biomass gasification, pyrolysis and torrefaction: practical design and theory*. 2018: Academic press.
6. Barisano, D., et al., *Investigation of an Intensified Thermo-Chemical Experimental Set-Up for Hydrogen Production from Biomass: Gasification Process Integrated to a Portable Purification System—Part II.* Energies, 2022. **15**(13): p. 4580.
7. Rey, J.R.C., et al., *A review of cleaning technologies for biomass-derived syngas.* Fuel, 2024. **377**: p. 132776.
8. Ahmad, A.A., et al., *Assessing the gasification performance of biomass: A review on biomass gasification process conditions, optimization and economic evaluation.* Renewable and Sustainable Energy Reviews, 2016. **53**: p. 1333–1347.
9. Mishra, S. and R.K. Upadhyay, *Review on biomass gasification: Gasifiers, gasifying mediums, and operational parameters.* Materials Science for Energy Technologies, 2021. **4**: p. 329–340.
10. Knoef, H.A.M.E., *Handbook Biomass gasification*. Second Edition ed. 2012, Netherlands: Biomass Technology Group (BTG).
11. Mayerhofer, M., et al., *Influence of pressure, temperature and steam on tar and gas in allothermal fluidized bed gasification.* Fuel, 2012. **99**: p. 204–209.
12. Pio, D., L. Tarelho, and M. Matos, *Characteristics of the gas produced during biomass direct gasification in an autothermal pilot-scale bubbling fluidized bed reactor.* Energy, 2017. **120**: p. 915–928.
13. Kim, Y.D., et al., *Air-blown gasification of woody biomass in a bubbling fluidized bed gasifier.* Applied energy, 2013. **112**: p. 414–420.
14. Ueki, Y., et al., *Gasification characteristics of woody biomass in the packed bed reactor.* Proceedings of the Combustion Institute, 2011. **33**(2): p. 1795–1800.
15. Kihedu, J.H., et al., *Counter-flow air gasification of woody biomass pellets in the auto-thermal packed bed reactor.* Fuel, 2014. **117**: p. 1242–1247.
16. Kihedu, J.H., R. Yoshiie, and I. Naruse, *Performance indicators for air and air–steam auto-thermal updraft gasification of biomass in packed bed reactor.* Fuel processing technology, 2016. **141**: p. 93–98.
17. Thomson, R., et al., *Clean syngas from small commercial biomass gasifiers; a review of gasifier development, recent advances and performance evaluation.* international journal of hydrogen energy, 2020. **45**(41): p. 21087–21111.
18. Pedroso, D.T., et al., *Experimental study of bottom feed updraft gasifier.* Renewable energy, 2013. **57**: p. 311–316.

19. Li, B., et al., *Characteristics of the temperature distribution and product gas evolving of an updraft biomass gasifier.* Energy & fuels, 2013. **27**(3): p. 1460–1465.

20. Couto, N.D., et al., *An experimental and numerical study on the Miscanthus gasification by using a pilot scale gasifier.* Renewable energy, 2017. **109**: p. 248–261.

21. Khan, Z., et al., *Design, instrumentation, and operation of a standard downdraft, laboratory-scale gasification testbed utilising novel seed-propagated hybrid Miscanthus pellets.* Applied Energy, 2022. **315**: p. 118864.

22. Wijekoon, W., et al., *Review and Prospects of Phytoremediation: Harnessing Biofuel-Producing Plants for Environmental Remediation.* Sustainability, 2025. **17**(3): p. 822.

23. Xue, G., et al., *Gasification of Miscanthus x giganteus in an Air-blown bubbling fluidized bed: a preliminary study of performance and agglomeration.* Energy & Fuels, 2014. **28**(2): p. 1121–1131.

24. Kallis, K.X., G.A.P. Susini, and J.E. Oakey, *A comparison between Miscanthus and bioethanol waste pellets and their performance in a downdraft gasifier.* Applied energy, 2013. **101**: p. 333–340.

25. Anicic, B., et al., *Agglomeration mechanism in biomass fluidized bed combustion–reaction between potassium carbonate and silica sand.* Fuel Processing Technology, 2018. **173**: p. 182–190.

26. Vakalis, S. and K. Moustakas, *Modelling of advanced gasification systems (MAGSY): Simulation and validation for the case of the rising co-current reactor.* Applied Energy, 2019. **242**: p. 526–533.

27. Weichselbaum, K., *Process and apparatus for thermochemical gasification of solid fuels.* Deutsches Patent- und Markenamt

DE102008043131B4, 2012.

28. Service, U.K.A., *Schedule of Accreditation: Accredited to ISO/IEC 17025:2017*. 2021, United Kingdom Accreditation Service.

29. CEN, C., *Biomass Gasification–Tar and Particles in Product Gases–Sampling and Analysis.* 2006.

30. Maschowski, C., et al., *Physicochemical and mineralogical characterization of biomass ash from different power plants in the Upper Rhine Region.* Fuel, 2019. **258**: p. 116020.

31. Rabea, K., et al., *Real-time performance investigation of a downdraft gasifier fueled by cotton stalks in a batch-mode operation.* Fuel, 2021. **300**: p. 120976.

32. Guo, F., et al., *Effect of design and operating parameters on the gasification process of biomass in a downdraft fixed bed: An experimental study.* International Journal of Hydrogen Energy, 2014. **39**(11): p. 5625–5633.

33. Rabea, K., et al., *An improved kinetic modelling of woody biomass gasification in a downdraft reactor based on the pyrolysis gas evolution.* Energy Conversion and Management, 2022. **258**: p. 115495.

34. Bandara, J.C., et al., *Air gasification of wood chips, wood pellets and grass pellets in a bubbling fluidized bed reactor.* Energy, 2021. **233**: p. 121149.

35. Gao, Y., et al., *Syngas production from biomass gasification: influences of feedstock properties, reactor type, and reaction parameters.* ACS omega, 2023. **8**(35): p. 31620–31631.

36. Pérez, J.F., A. Melgar, and P.N. Benjumea, *Effect of operating and design parameters on the gasification/combustion process of waste biomass in fixed bed downdraft reactors: An experimental study.* Fuel, 2012. **96**: p. 487–496.

37. Li, X., et al., *Solar-driven gasification in an indirectly-irradiated thermochemical reactor with a clapboard-type internally-circulating fluidized bed.* Energy Conversion and Management, 2021. **248**: p. 114795.

38. Cortazar, M., et al., *A comprehensive review of primary strategies for tar removal in biomass gasification.* Energy Conversion and management, 2023. **276**: p. 116496.

39. Giechaskiel, B. and M. Clairotte, *Fourier transform infrared (FTIR) spectroscopy for measurements of vehicle exhaust emissions: A review.* Applied Sciences, 2021. **11**(16): p. 7416.

40. Morris, J.D., S.S. Daood, and W. Nimmo, *The use of kaolin and dolomite bed additives as an agglomeration mitigation method for wheat straw and miscanthus biomass fuels in a pilot-scale fluidized bed combustor.* Renewable Energy, 2022. **196**: p. 749–762.

41. Pio, D., et al., *Low-cost catalysts for in-situ improvement of producer gas quality during direct gasification of biomass.* Energy, 2018. **165**: p. 442–454.

42. Liu, L., et al., *Experimental study of biomass gasification with oxygen-enriched air in fluidized bed gasifier.* Science of The Total Environment, 2018. **626**: p. 423–433.

43. Nikolaidis, P. and A. Poullikkas, *A comparative overview of hydrogen production processes.* Renewable and Sustainable Energy Reviews, 2017. **67**: p. 597–611.

44. Jayathilake, R. and S. Rudra, *Numerical and experimental investigation of Equivalence Ratio (ER) and feedstock particle size on birchwood gasification.* Energies, 2017. **10**(8): p. 1232.

45. Meng, F., J. Meng, and D. Zhang, *Influence of higher equivalence ratio on the biomass oxygen gasification in a pilot scale fixed bed gasifier.* Journal of Renewable and Sustainable Energy, 2018. **10**(5).

46. Reinmöller, M., et al., *Formation and transformation of mineral phases in biomass ashes and evaluation of the feedstocks for application in high-temperature processes.* Renewable Energy, 2023. **210**: p. 627–639.

47. Nor Aznizam Nik Norizam, N., et al., *Impact of the blending of kaolin on particulate matter (PM) emissions in a biomass field-scale 250 kW grate boiler.* Fuel, 2024. **374**: p. 132454.

48. *95/00598 Understanding slagging and fouling during pf combustion.* Fuel and energy abstracts, 1995. **36**(1): p. 35–35.

49. Fatehi, H., et al., *Modeling of alkali metal release during biomass pyrolysis.* Proceedings of the Combustion Institute, 2017. **36**(2): p. 2243–2251.

50. Cao, W., et al., *Prediction of potassium compounds released from biomass during combustion.* Applied Energy, 2019. **250**: p. 1696–1705.